Supplementary information for

Weak-coupling to strong-coupling quantum criticality crossover in a Kitaev quantum spin liquid α-$RuCl_3$

Jae-Ho Han*, Seung-Hwan Do*, Kwang-Yong Choi, Sang-Youn Park, Jae-You Kim, Sungdae Ji†, Ki-Seok Kim‡, and Jae-Hoon Park§

* These authors contributed equally to this work

† jsungdae@kaeri.re.kr

‡ tkfkd@postech.ac.kr

§ jhp@postech.ac.kr

Table of Contents

Supplementary Methods **3**

A. Experimental details 3

B. Comparion between inelastic neutron scattering and theortical models 3

C. ac-magnetic susceptibility measurement with fields along [0,1,0] and [0,0,1] directions 4

D. Specific heat of α-$RuCl_3$ 5

Supplementary Notes **7**

A. Effective field theory, renormalization group analysis, and dynamic spin susceptibility for the high-energy weak-coupling fixed point 7

B. Effective field theory, dynamic spin susceptibility, specific heat, and dynamical mean-field theory analysis for the low-energy strong-coupling fixed point 18

C. Calculation details 22

Supplementary References **27**

Supplementary Methods

A. Experimental details

Single crystalline α-$RuCl_3$ samples were prepared using the vacuum sublimation method as described in the previous study [1]. The crystal orientation was determined by using the X-ray Laue. The magnetization and specific heat of $RuCl_3$ were measured by using the conventional vibrating sample magnetometry (VSM) and calorimeter equipped at a commercial Quantum Design Physical Property Measurement System (PPMS-Dynacool), respectively. The specific heat results are displayed in Supplementary Figure 4.

Zero-field INS measurements were performed by using MERLIN and LET time-of-flight spectrometers at the ISIS spallation neutron source in Rutherford Appleton Laboratory, UK. 165 pieces of α-$RuCl_3$ single crystals with the total mass ~ 5.5 g were co-aligned on an aluminum plate with the (0 K L) scattering plane. The samples were placed under a liquid helium flow-type cryostat with the temperature control ranging from 2 K to 290 K. In the MELRIN experiments, we used a chopper frequency of 300 Hz, which provides $E_{\mathrm{i}} = 12$ meV, 22 meV, and 50 meV of incident neutron energies with FWHM (full width at the half maximum) energy resolutions of 0.34 meV, 0.75 meV, and 2.23 meV at elastic scattering, respectively. The measurements were performed for the sample rotation from -52° to 52° with 4° step referring to 0° at $k_i \parallel c^*$. The LET experiments were performed at E_i = 10 meV with the energy resolution of 0.36 meV (FWHM) for the elastic scattering, and the sample rotation from -30° to 30° with 5° step relative to $k_i \parallel c^*$. The background signals were separately obtained by using an identical aluminum sample holder both in the MERLIN and LET experiments for the background correction. INS data were normalized, and converted to the unit for the neutron scattering function by using the incoherent neutron scattering intensity of a standard reference vanadium sample.

The data presented in Figs. 5 and 6 in the main text were obtained by integration over [0, 0, L] = [-2.5, 2.5], [0, K, 0] = [-0.17, 0.17], and [H, -0.5H, 0] = [-0.17, 0.17]. The magnetic form factor contribution from the L-component in the integrated data was corrected by dividing with the Ru^{3+} magnetic form factor at each data point [1], and the scaled data were compared with the theoretical model calculations for $S(\Gamma, \omega)$. All the data were analyzed by using HORACE software distributed by ISIS [2].

B. Comparion between inelastic neutron scattering and theortical models

Supplementary Figure 1a shows neutron scattering functions $S(\mathbf{Q}, \omega)$ for $\mathbf{Q} = \Gamma$ (0, 0, 0) at temperatures T = 2.3 K, 25 K, and 75 K. The data exhibit the continuum excitations emerging on cooling across T_{H} (~ 100 K), and the continuum still remains even below T_{N} ~ 6.5 K. The experimental $S(\Gamma, \omega)$s are compared with the theoretical spectra in the linear-linear scale. The theoretical spectra, which are separately extracted from two different models, the weak coupling model (Eq. (19) in the main text) and strong coupling model (Eq. (21) in the main text), are presented by blue and red lines in the high and low energy ranges of 4 meV $\leq \hbar\omega \leq$ 15 meV and 1 meV $\leq \hbar\omega \leq$ 5 meV, respectively. The models well reproduce the respective overall line shapes of $S(\Gamma, \omega)$s in both energy ranges except additional contributions, which are not included in the model spectra. In the comparison for $S(\Gamma, \omega)$ at T = 2.3 K (blow T_{N}), we only present the weak coupling model spectrum in the high energy range since $S(\Gamma, \omega)$ in the low energy range is strongly disturbed by the apparent AFM spin wave excitations, which are not taken into account in the spectrum of the low energy strong coupling model. A broad peak, which involves the AFM multi-magnon modes, also appears around 14 meV. The spectral weight of the multi-magnon contribution was simply formulated with a phenomenological Gaussian function (red solid line) as shown in the left first figure. The phonon contribution, which increases upon heating, also appears as an additional sharp peak at $\hbar\omega \simeq 6$ meV [1, 3], and causes a deviation from the weak coupling model.

Supplementary Figure 1b presents a detailed comparison of the $S(\Gamma, \omega)$s in the low energy region, 1 meV $\leq \hbar\omega \leq$ 5 meV, with the strong coupling model. The calculated spectra from the strong coupling model reproduce the $S(\Gamma, \omega)$s at different temperatures above T_{N} up to 125 K.

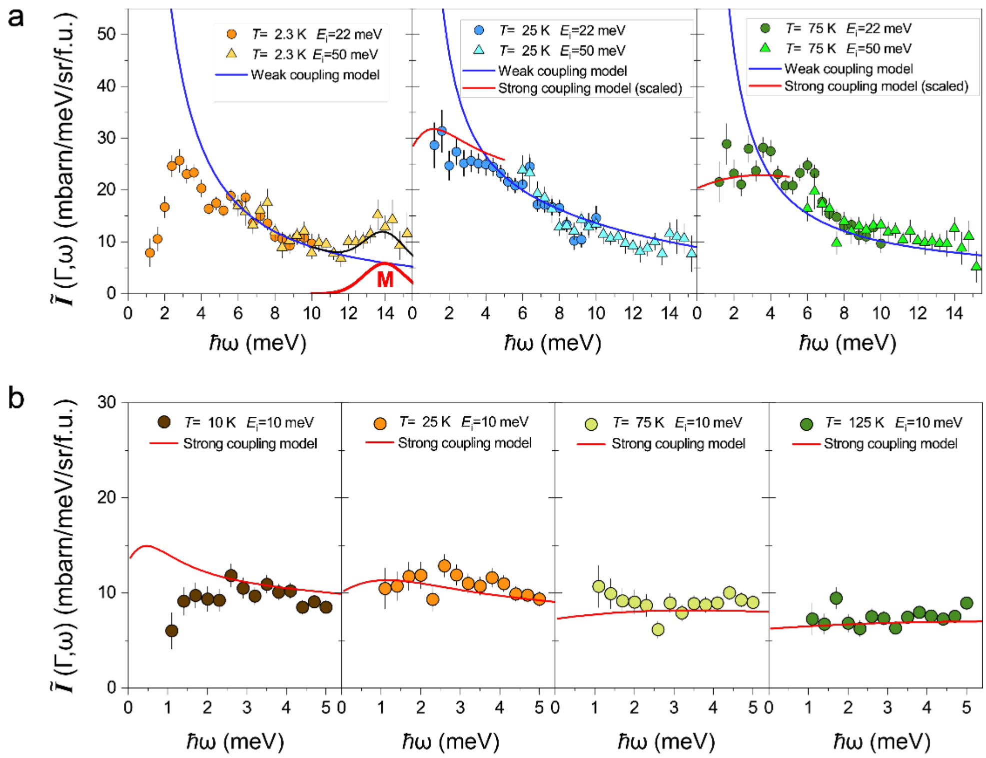

Supplementary Figure 1. Comparison of the inelastic neutron scattering with the theoretical models. a Neutron scattering function $S(\Gamma,\omega)$s measured from MERLIN experiment by using E_{i} = 22 meV and 50 meV, with integration over [0,0,L]=[-2.5, 2.5], [0,K,0]= [-0.17,0.17], and [H,-0.5H,0]=[-0.17,0.17]. The theoretical scaling functions are extracted from the weak coupling model (blue line) for a high energy scale of 4 meV ≤ $\hbar\omega$ ≤ 15 meV and the strong coupling (red line) for a low energy scale of 0 meV ≤ $\hbar\omega$ ≤ 5 meV. Below T_{N} (2.3 K), only the high energy weak coupling model is presented in the figure since the low energy excitations are dominated by the AFM spin wave excitations which are not taken into account in the low energy strong coupling model. The AFM multi-magnon contributions (red solid line), marked with 'M', are presented by a Gaussian function centered at 14 meV. **b** $S(\Gamma, \omega)$ from LET experiment using E_i = 10 meV, integrated over [0,0,L]=[-2.5,2.5], [0,K,0]= [-0.17,0.17], and [H,-0.5H,0]=[-0.17,0.17]. The obtained data (filled circle) are compared with the strong coupling model (solid red line).

C. ac-magnetic susceptibility measurement with fields along [0,1,0] and [0,0,1] directions.

Supplementary Figure 2a shows the real part of the ac-magnetic susceptibility $\chi'_{\mathrm{ac}}(T,H)$ measured with external magnetic fields along H//[0,1,0]. For this field direction, the ac-magnetic susceptibility at T=1.8 K shows a sharp single peak around 7 T, indicating a phase transition from zigzag antiferromagnet to polarized ferromagnet (PF). Figure 7b in the main text shows the measured $\chi'_{\mathrm{ac}}(T)$ curves with varying external magnetic fields near the antiferromagnetic phase boundary. Noticeably, similar to $\chi'_{\mathrm{ac}}(T)$ for H//[-2,1,0] (see Fig.7 of the main text), ac susceptibility at H_{C}~7.8 T reveals a power-law behavior in the temperature range 3 K≤ T ≤ 12 K. The scaling plot for $\chi'_{\mathrm{ac}}T^{\alpha}$ with α = 0.14 is presented in Fig. 2c, showing the collapses of the quantities in a single line as a function $(H-H_{\mathrm{C}})/k_{\mathrm{B}}T$ above H_{C} = 7.8 T.

On the other hand, in the magnetic field along the [0,0,1] direction (c-axis), the zigzag antiferromagnetic phase is robust up to 30 T [4]. Therefore, χ'_{ac} measured for H//[0,0,1] does not show any phase boundary or scaling behavior up to 14T, which is the highest magnetic field in our data. This large magnetic anisotropy in α-$RuCl_3$ is attributed to the symmetric anisotropic exchange (termed Γ) [5], and precedent DFT calculations and experimental analysis (for recent summary, Table 1 in [6]) showed that the size of the term is not small in this compound.

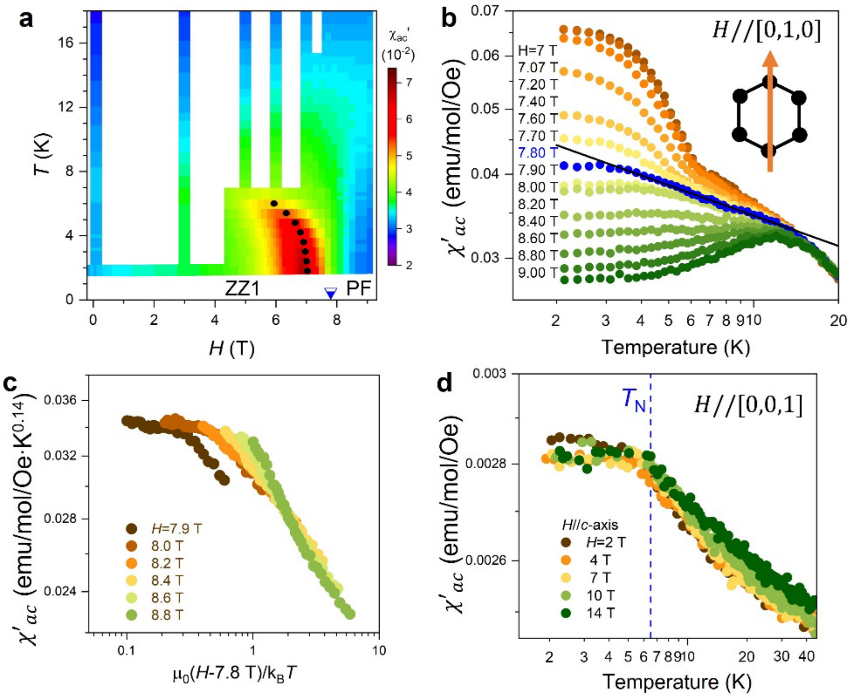

Supplementary Figure 2. ac-magnetic susceptibility with external magnetic fields along [0,1,0] and [0,0,1]. a Temperature-magnetic field contour plot of the ac-magnetic susceptibility for external magnetic field along honeycomb bond direction (see the inset of b). The black circles indicate the phase boundaries between zigzag AFM and polarized ferromagnet (PF). **b** $\chi'_{\mathrm{ac}}(T)$ measured at various fields near the phase boundary of AFM, displayed in log-log plot. **c** A scaled plot of the $\chi'_{\mathrm{ac}}T^{\alpha}$ with $\alpha = 0.14$ as a function of $(H - 7.8\ \mathrm{T})/k_{\mathrm{B}}T$. **d** $\chi'_{\mathrm{ac}}(T)$ measured with external fields along [0,0,1]. The blue dashed line indicates the AFM transition temperature at zero magnetic field.

D. Specific heat of α-$RuCl_3$

To study the thermodynamic behavior of α-$RuCl_3$, we performed specific heat (C_P) measurements the single crystalline sample. Supplementary Figure 3a shows the temperature dependence from 1.8 K to 200 K at $H = 0$ T and Supplementary Figure 3b does the temperature dependence in a 1.8 K to 25 K window for different H-fields ($H \parallel [2\ \bar{1}\ 0]$) ranging from 0 T to 9 T. The specific heat C_P of α-$RuCl_3$ consists of magnetic (C_{mag}) and lattice (C_L) contributions. C_L, which is presented by a red solid line in both figures, was estimated from C_P of a non-magnetic iso-structural compound $ScCl_3$ with Debye temperature scaling [7]. Supplementary Figure 3c displays the field dependent magnetic specific heat C_{mag} obtained by subtracting C_L from C_P ($C_{\mathrm{mag}} = C_P - C_L$) of α-$RuCl_3$.

The zero-field C_{mag} shows a sharp peak at $T_N \simeq 6.5$ K, and exhibits the plateau behavior above T_N as expected in the local quantum critical region described in the main text. With increasing magnetic field, the peak position and height gradually decrease, and the peak disappears across $H_C \simeq 6$ T. We note that the transition temperature $T_N(H)$ is not well defined at 6 T near the critical field.

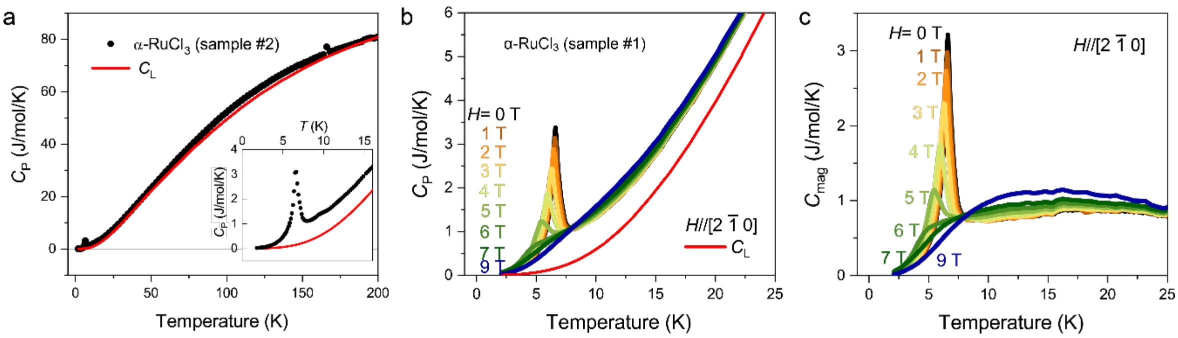

Supplementary Figure 3. Specific heat measurements in magnetic fields. a Specific heat of α-$RuCl_3$ and the lattice contribution C_L (red solid line) estimated from $ScCl_3$. Inset shows a magnification of specific heats at a low temperature region. A black arrow indicates the AFM transition peak at $T_N \simeq 6.5$ K. **b** Specific heat of α-$RuCl_3$ for different H-fields along $[2,\bar{1},0]$ ranging from 0 to 9 T. C_L is presented by a red solid line again. **c** Magnetic specific heat of α-$RuCl_3$ for the different H-fields.

Supplementary Notes

A. Effective field theory, renormalization group analysis, and dynamic spin susceptibility for the high-energy weak-coupling fixed point

1. Construction of an effective field theory

In order to construct an effective field theory, we start from a ferromagnetic Kitaev Hamiltonian [8]

$$\begin{aligned} H_{\mathrm{K}} &= -K_x \sum_{x-\mathrm{bond}} \sigma_i^x \sigma_j^x - K_y \sum_{y-\mathrm{bond}} \sigma_i^y \sigma_j^y - K_z \sum_{z-\mathrm{bond}} \sigma_i^z \sigma_j^z \\ &= -K_x \sum_r \sigma_{r,\mathrm{w}}^x \sigma_{r+x,\mathrm{b}}^x - K_y \sum_r \sigma_{r+y,\mathrm{b}}^y \sigma_{r,\mathrm{w}}^y - K_z \sum_r \sigma_{r,\mathrm{b}}^z \sigma_{r,\mathrm{w}}^z, \end{aligned} \tag{1}$$

Here local spins satisfy the commutation relation $[\sigma_i^\alpha, \sigma_j^\beta] = 2i\epsilon_{\alpha\beta\gamma}\sigma_i^\gamma \delta_{ij}$. The lattice vector is given by $r = n_x a_x + n_y a_y$ with $n_x, n_y \in \mathbb{Z}$, where the lattice unit cell is spanned by $a_x = a(\sqrt{3}/2, 3/2)$ and $a_y = a(-\sqrt{3}/2, 3/2)$ for the hexagonal bond length a. The subscripts w and b represent two triangular sublattices as shown in Supplementary Figure 4a (white and black filled circles).

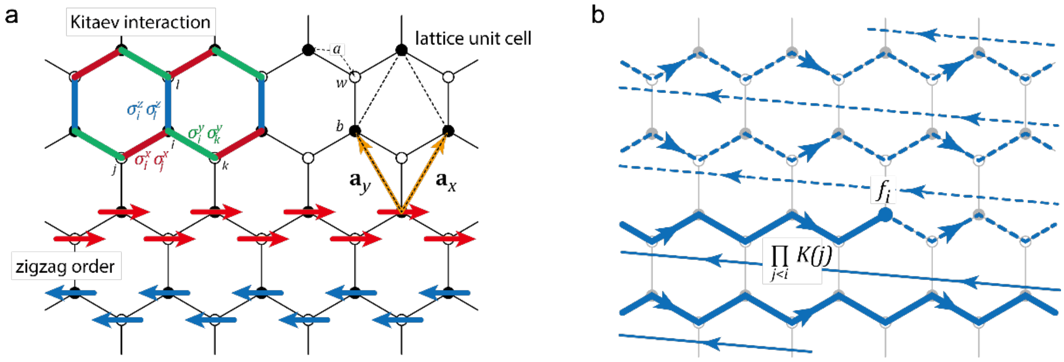

Supplementary Figure 4. Schematic figure of the model. a Honeycomb lattice, Kitaev interaction, zigzag antiferromagnetic order, lattice and basis, and lattice unit cell. **b** Order of lattice points.

Now we introduce zigzag AFM ordering observed below T_{N} in α-$\mathrm{RuCl_3}$ as shown in Supplementary Figure 4a [9, 10, 11, 12]. This AFM order likely results from the interplay among Kitaev, Heisenberg, and ansiotrpic spin exchange interactions on the honeycomb lattice. Here, we implement a zigzag AFM fixed point in the Kitaev spin liquid state and investigate emergent physics near this conjectured fixed point. The corresponding effective Hamiltonian, which represents the coupling between the zigzag AFM fluctuation and Kitaev spins, can be given by

$$H_{\mathrm{ZZ}} = -g \sum_i \phi_i \sigma_i^z, \tag{2}$$

where $\phi_i = \langle \sigma_i^z \rangle$ and g is an effective coupling constant. In the zigzag AFM phase, ϕ_i become finite with $\phi_{r,w} = -\phi_{r,b}$.

In order to describe the Kitaev spin liquid phase, we make the Jordan-Wigner (JW) transformation [13, 14]

$$\sigma_i^z = 2f_i^\dagger f_i - 1, \qquad \sigma_i^+ = \frac{1}{2}(\sigma_i^x + \mathrm{i}\sigma_i^y) = \left(\prod_{j<i} K(j)\right) f_i^\dagger, \sigma_i^- = \frac{1}{2}(\sigma_i^x - \mathrm{i}\sigma_i^y) = \left(\prod_{j<i} K(j)\right) f_i, \tag{3}$$

where $K(j) = 2f_j^\dagger f_j - 1$ and the order of lattice points is shown in Supplementary Figure 4b. Here, the spinless fermion field represents a domain wall excitation, where the nonlocal string operator implies a topological defect [15]. It is straightforward to check out $[\sigma_i^z, \sigma_j^\pm] = \pm 2\sigma^\pm \delta_{ij}$, $[\sigma_i^+, \sigma_j^-] = \sigma_i^z \delta_{ij}$ for spin operators and $\{f_i^\dagger, f_j\}=\delta_{ij}$, $\{f_i, f_j\}=\{f_i^\dagger, f_j^\dagger\}=0$ for the JW fermions. This nonlocal transformation makes us to rewrite Kitaev and AFM Ising spin interaction terms as follows;

$$\begin{aligned} H_{\mathrm{K}} = -K_x \sum_r (f_{r+x,\mathrm{b}}^\dagger + f_{r+x,\mathrm{b}})(f_{r,\mathrm{w}}^\dagger - f_{r,\mathrm{w}}) - K_y \sum_r (f_{r+y,\mathrm{b}}^\dagger + f_{r+y,\mathrm{b}})(f_{r,\mathrm{w}}^\dagger - f_{r,\mathrm{w}}) \\ - K_z \sum_r (2f_{r,\mathrm{b}}^\dagger f_{r,\mathrm{b}} - 1)(2f_{r,\mathrm{w}}^\dagger f_{r,\mathrm{w}} - 1), \end{aligned} \tag{4}$$

$$H_{\mathrm{ZZ}} = -g \sum_r \left[\phi_{r,\mathrm{w}}(2f_{r,\mathrm{w}}^\dagger f_{r,\mathrm{w}} - 1) + \phi_{r,b}(2f_{r,\mathrm{b}}^\dagger f_{r,\mathrm{b}} - 1)\right]. \tag{5}$$

The Kitaev Hamiltonian can be diagonalized by introducing two complex fermions, which correspond to mixtures of fermions on two sites (black and white) linked by the directional z-bond in Supplementary Figure 4a, defined as [13]

$$\chi_r = \mathrm{Re}f_{r,\mathrm{w}} - \mathrm{i}\mathrm{Im}f_{r,\mathrm{b}}, \quad \psi_r = \mathrm{Im}f_{r,\mathrm{w}} + \mathrm{i}\mathrm{Re}f_{r,\mathrm{b}}. \tag{6}$$

Then the Kitaev and coupling Hamiltonians are presented by

$$\begin{aligned} H_{\mathrm{K}} = -K_x \sum_r (\psi_{r+x}^\dagger - \psi_{r+x})(\psi_r^\dagger + \psi_r) - K_y \sum_r (\psi_{r+y}^\dagger - \psi_{r+y})(\psi_r^\dagger + \psi_r) \\ + K_z \sum_r (2\chi_r^\dagger \chi_r - 1)(2\psi_r^\dagger \psi_r - 1), \end{aligned} \tag{7}$$

$$H_{\mathrm{ZZ}} = -\mathrm{i}g \sum_r \phi_r(\psi_r^\dagger \chi_r^\dagger + \psi_r \chi_r), \tag{8}$$

where we set $\phi_{r,w} = -\phi_{r,b} \equiv \phi_r/2$. Here $\chi_r^\dagger \chi_r$ can be recognized to be a conserved quantity, *i.e.*, $[\chi_r^\dagger \chi_r, H_K] = 0$, in the absence of zigzag AFM fluctuations. This conservation identifies $\chi_r^\dagger \chi_r$ with the Z_2 flux density, described by localized Majorana fermions in the original Kitaev model. As a result, the ground state of the Kitaev Hamiltonian is described by $\chi_r^\dagger \chi_r = 0$. Within this sector, the Kitaev Hamiltonian becomes reduced into a same form as the *p-wave* superconductivity of chargeless spinons

$$\begin{aligned} H_{\mathrm{K}} &= -K_x \sum_r (\psi_{r+x}^\dagger - \psi_{r+x})(\psi_r^\dagger + \psi_r) - K_y \sum_r (\psi_{r+y}^\dagger - \psi_{r+y})(\psi_r^\dagger + \psi_r) \\ &\quad - K_z \sum_r (2\psi_r^\dagger \psi_r - 1) \\ &= \sum_k \epsilon_k \psi_k^\dagger \psi_k + \sum_k \frac{\mathrm{i}\Delta_k}{2}(\psi_k^\dagger \psi_{-k}^\dagger + \psi_k \psi_{-k}). \end{aligned} \tag{9}$$

Here, the energy dispersion relation is given by $\epsilon_k = -2K_z - 2K_x \cos k \cdot a_x - 2K_y \cos k \cdot a_y$ and the *p-wave* pairing amplitude becomes $\Delta_k = 2K_x \sin k \cdot a_x + 2K_y \sin k \cdot a_y$, where both a_x and a_y span the lattice unit cell as discussed before. ψ_k is the Fourier transform of ψ_r-field given by $\psi_r = \frac{1}{\sqrt{N_z}} \sum_k \mathrm{e}^{\mathrm{i}k\cdot r} \psi_k$, where N_z is the number of z-bonds or the number of triangular Bravais lattice sites in the honeycomb lattice.

Performing the Bogoliubov transformation of $\gamma_k = u_k \psi_k + v_k \psi_{-k}^\dagger$, where the coherence factors of $u_{-k} = u_k$

and $v_{-k} = -v_k$ satisfy $|u_k|^2 + |v_k|^2 = 1$, we found that the quasiparticle spectrum is given by $E_k = \sqrt{\epsilon_k^2 + \Delta_k^2}$ [13]. It turns out that gapless points arise at $k = \pm k_0$ with $k_0 = \frac{1}{3}b_x - \frac{1}{3}b_y$ in the symmetric case of $K_x = K_y = K_z \equiv K$, where the reciprocal lattice vectors are given by $b_x = 2\pi a(1/\sqrt{3}, 1/3)$, $b_y = 2\pi a(-1/\sqrt{3}, 1/3)$. See Supplementary Figure 5.

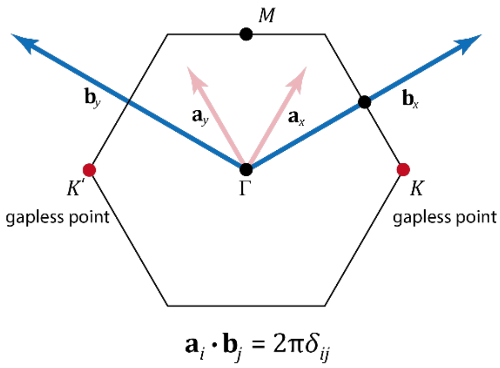

Supplementary Figure 5. Brillouin zone and gapless points. The red points shows two gapless points K ($\mathbf{k} = \mathbf{k}_0$) and K' ($\mathbf{k} = -\mathbf{k}_0$) in the Brillouin zone.

Taking into account zigzag AFM fluctuations described by ϕ_r, $\chi_r^\dagger \chi_r$ is not a conserved quantity any more. Hereafter, we only consider the symmetric case, $K_x = K_y = K_z \equiv K$, and the effective Hamiltonians become

$$H_{\mathrm{K}} = \sum_k \epsilon_k \psi_k^\dagger \psi_k + \sum_k \frac{\mathrm{i}\Delta_k}{2}\left(\psi_k^\dagger \psi_{-k}^\dagger + \psi_k \psi_{-k}\right) + 2K \sum_k \chi_k^\dagger \chi_k + \frac{4K}{N_z} \sum_{k,p,q} \chi_p^\dagger \chi_{p+q} \psi_{k+q}^\dagger \psi_k \tag{10}$$

$$H_{\mathrm{ZZ}} = -\mathrm{i}g \sum_{k,q} \phi_q \left(\chi_{-k+q}^\dagger \psi_k^\dagger + \psi_k \chi_{-k-q}\right), \tag{11}$$

where χ_k and ϕ_k are the Fourier transformations as $\chi_r = \frac{1}{\sqrt{N_z}} \sum_k \mathrm{e}^{\mathrm{i}k\cdot r} \chi_k$ and $\phi_r = \sum_k \mathrm{e}^{\mathrm{i}k\cdot r} \phi_k$, and an irrelevant constant term is eliminated. We note that $\phi_q^\dagger = \phi_{-q}$, where ϕ_r is real.

In order to construct an effective field theory, we consider low energy states near the gapless points and obtain

$$\begin{aligned} H_{\mathrm{K}} &= \sum_k \left(\epsilon_{+,k} \psi_{+,k}^\dagger \psi_{+,k} + \epsilon_{-,k} \psi_{-,k}^\dagger \psi_{-,k}\right) \\ &+ \sum_k \left\{\frac{\mathrm{i}\Delta_{+,k}}{2}\left(\psi_{+,k}^\dagger \psi_{-,-k}^\dagger + \psi_{+,k}\psi_{-,-k}\right) + \frac{\mathrm{i}\Delta_{-,k}}{2}\left(\psi_{-,k}^\dagger \psi_{+,-k}^\dagger + \psi_{-,k}\psi_{+,k}\right)\right\} \\ &+ 2K \sum_k \left(\chi_{+,k}^\dagger \chi_{+,k} + \chi_{-,k}^\dagger \chi_{-,k}\right) \\ &+ \frac{4K}{N_z} \sum_{k,p,q} \left(\chi_{+,p}^\dagger \chi_{+,p+q} + \chi_{-,p}^\dagger \chi_{-,p+q}\right)\left(\psi_{+,k+q}^\dagger \psi_{+,k} + \psi_{-,k+q}^\dagger \psi_{-,k}\right) \\ &+ \frac{4K}{N_z} \sum_{k,p,q} \left(\chi_{+,p}^\dagger \chi_{-,p+q} + \chi_{-,p}^\dagger \chi_{+,p+q}\right)\left(\psi_{+,k+q}^\dagger \psi_{-,k} + \psi_{-,k+q}^\dagger \psi_{+,k}\right), \end{aligned} \tag{12}$$

$$H_{\mathrm{ZZ}} = -\mathrm{i}g \sum_{k,q} \phi_q \left(\chi_{-k+q}^{\dagger} \psi_k^{\dagger} + \psi_k \chi_{-k-q} \right), \tag{13}$$

where $\epsilon_{\pm,k} \approx \pm v k_x$ and $\Delta_{\pm,k} \approx -v k_y$ with $v = 3Ka$.

Considering two-component Dirac spinors of

$$\Psi_k = \begin{pmatrix} \psi_{+,k} \\ \psi_{-,-k}^{\dagger} \end{pmatrix}, \quad X_k = \begin{pmatrix} \chi_{+,k} \\ \chi_{-,-k}^{\dagger} \end{pmatrix}, \tag{14}$$

we reformulate the effective Hamiltonian as follows

$$H_{\mathrm{K}} = \sum_k \Psi_k^{\dagger} \left(v k_x \tau^z + v k_y \tau^y \right) \Psi_k + 2K \sum_k X_k^{\dagger} \tau^z X_k + H_{\mathrm{I}}, \tag{15}$$

$$H_{\mathrm{ZZ}} = -\mathrm{i}g \sum_{k,q} \phi_q \left(X_{k+q}^{\dagger} \tau^x \Psi_k - \Psi_k^{\dagger} \tau^x X_{k-q} \right), \tag{16}$$

where H_{I} represents four-fermion interactions between itinerant and localized fermions. It turns out that these effective interactions are not relevant in the renormalization group (RG) sense, which will be discussed below. Then, the effective action is given by

$$\begin{aligned} S = \int \frac{d^3k}{(2\pi)^3} \, \bar{\Psi}(k) \, \mathrm{i}\gamma \cdot k \, \Psi(k) + \int \frac{d^3k}{(2\pi)^3} \, \bar{X}(k) (\mathrm{i}\gamma_0 k_0 + \mathrm{i}\gamma_1 M_X) X(k) + S_{\mathrm{I}} \\ -\mathrm{i}g \int \frac{d^3k d^3q}{(2\pi)^6} \left(\bar{X}(k+q) \Psi(k) - \bar{\Psi}(k) X(k-q) \right) \phi(q), \end{aligned} \tag{17}$$

where $\bar{\Psi}(k) = \Psi^{\dagger}(k)\gamma_0$ and $\bar{X}(k) = X^{\dagger}(k)\gamma_0$. Dirac gamma matrices are $\gamma_0 = \sigma^x$, $\gamma_1 = -\sigma^y$, and $\gamma_2 = \sigma^z$. S_{I} is the action term corresponding to H_{I}. The excitation gap for the Z_2-flux fluctuations is $M_X = 2K$ and the interaction strength between itinerant and localized fermionic spinons (S_{I}) is $4K$. It is rather unexpected to see that the gap of localized spinon excitations appears with the γ_1 matrix, which implies that M_X plays the role of an effective gauge field to generate the spinon current $\mathrm{i}\bar{X}(k)\gamma_1 X(k)$.

It is natural to introduce an effective action S_{ϕ} for the dynamics of zigzag AFM fluctuations into the above effective action, and S_{ϕ} is given by

$$S_{\phi} = \frac{1}{2} \int \frac{d^3k}{(2\pi)^3} \, \phi(-k)(k^2 + r)\phi(k) + \frac{\lambda}{4!} \int \frac{d^3k d^3p d^3q}{(2\pi)^9} \, \phi(-k)\phi(k+q)\phi(-p-q)\phi(p). \tag{18}$$

Here, r is an effective mass parameter and λ is an effective self-interaction constant. This ϕ^4-theory is an effective field theory in an Ising AFM lattice model [16].

Through the g-vertex, critical fluctuations of the ϕ-fields generate a kinetic term of the X-field. Including this kinetic term, we construct the partition function in an effective field theory as

$$\begin{aligned} Z_{\mathrm{eff}} &= \int D\Psi(k) DX(k) D\phi(k) \exp(-S_{\mathrm{eff}}[\Psi(k), X(k), \phi(k)]) \\ S_{\mathrm{eff}}[\Psi(k), X(k), \phi(k)] &= \int \frac{d^3k}{(2\pi)^3} \, \bar{\Psi}(k) \mathrm{i}\gamma \cdot k \Psi(k) + \int \frac{d^3k}{(2\pi)^3} \, \bar{X}(k) \mathrm{i}\gamma \cdot (k + M) X(k) \\ &\quad -\mathrm{i}g \int \frac{d^3k d^3q}{(2\pi)^6} \, \phi(q) \left(\bar{X}(k+q) \Psi(k) - \bar{\Psi}(k) X(k-q) \right) \\ &\quad + \frac{1}{2} \int \frac{d^3k}{(2\pi)^3} \, \phi(-k)(k^2 + r)\phi(k) + \frac{\lambda}{4!} \int \frac{d^3k d^3p d^3q}{(2\pi)^9} \phi(-k)\phi(k+q)\phi(-p-q)\phi(p). \end{aligned} \tag{19}$$

Here, we neglect the four-fermion interaction term since it is irrelevant in RG sense [17]. Also we set the velocities of two fields be identical because the Dirac theory recovers the Lorentz symmetry as it flows to the low-energy limit in RG [18]. It is interesting to observe that the gapless point of being-itinerant spinons $X(k)$ is separated from that of $\Psi(k)$ in an amount of $M = (0, M_X, 0)$ in the momentum space. This means that Z_2 flux fluctuations driven by zigzag AFM excitations are represented by a current-flowing state in the Kitaev spin liquid phase.

2. Wilsonian renormalization group analysis

We rewrite the effective action in a D-dimension with a cutoff Λ as

$$\begin{aligned} S = &\int_\Lambda \frac{d^D k}{(2\pi)^D} \bar{\Psi}(k) \mathrm{i}\gamma \cdot k \Psi(k) + \int_\Lambda \frac{d^D k}{(2\pi)^D} \bar{X}(k) \mathrm{i}\gamma \cdot (k + M) X(k) \\ &- \mathrm{i}g \int_\Lambda \frac{d^D k d^D q}{(2\pi)^{2D}} \left(\bar{X}(k+q)\Psi(k) - \bar{\Psi}(k) X(k-q)\right)\phi(q) \\ &+ \frac{1}{2}\int_\Lambda \frac{d^D k}{(2\pi)^D} k^2 \phi(-k)\phi(k) + \frac{\lambda}{4!}\int_\Lambda \frac{d^D k d^D p d^D q}{(2\pi)^{3D}} \phi(-k)\phi(k+q)\phi(-p-q)\phi(p). \end{aligned} \tag{20}$$

In order to perform the Wilsonian RG analysis, we separate all field variables into low and high energy-momentum parts

$$\begin{aligned} \Psi(k) &= \Psi(k)\Theta\left[k\left(\frac{\Lambda}{b} - k\right)\right] + \Psi(k)\Theta\left[(\Lambda - k)\left(k - \frac{\Lambda}{b}\right)\right] \equiv \Psi_{\mathrm{L}}(k) + \Psi_{\mathrm{H}}(k), \\ X(k) &= X(k)\Theta\left[k\left(\frac{\Lambda}{b} - k\right)\right] + X(k)\Theta\left[(\Lambda - k)\left(k - \frac{\Lambda}{b}\right)\right] \equiv X_{\mathrm{L}}(k) + X_{\mathrm{H}}(k), \\ \phi(k) &= \phi(k)\Theta\left[k\left(\frac{\Lambda}{b} - k\right)\right] + \phi(k)\Theta\left[(\Lambda - k)\left(k - \frac{\Lambda}{b}\right)\right] \equiv \phi_{\mathrm{L}}(k) + \phi_{\mathrm{H}}(k). \end{aligned} \tag{21}$$

Here, $k = \sqrt{\sum_{\mu=0}^{d} k_\mu^2}$ in the Euclidean signature and b is a scaling parameter to define the observation energy scale. $\Theta(x)$ is a step function with $\Theta(x) = 1$ for $x \geq 0$ and $\Theta(x) = 0$ for $x < 0$.

Implementing these expressions into the effective field theory, we can divide the action into three parts: low-energy field action S_{L}, high-energy field action S_{H}, and terms of mixed fields. Integrating over high energy degrees of freedom, *i.e.*, performing the functional integral of $\int D\Psi_{\mathrm{H}}(k) D X_{\mathrm{H}}(k) D\phi_{\mathrm{H}}(k)$ in the perturbative way of the cumulant expansion, we obtain quantum-fluctuation corrections on the dynamics of low energy degrees of freedom. While many new interaction terms of low-energy fields arise, we are interested in the same form of terms in the original action. Then the corrections are of a form

$$\begin{aligned} \delta S = &\int_{\Lambda/b} \frac{d^D k}{(2\pi)^D} \delta_\Psi \bar{\Psi}_{\mathrm{L}}(k) \mathrm{i}\gamma \cdot k \Psi_{\mathrm{L}}(k) + \int_{\Lambda/b} \frac{d^D k}{(2\pi)^D} \bar{X}_{\mathrm{L}}(k) \mathrm{i}\gamma \cdot (\delta_X k + \delta_M M) X_{\mathrm{L}}(k) \\ &- \mathrm{i}g\delta_g \int_{\Lambda/b} \frac{d^D k d^D q}{(2\pi)^{2D}} \left(\bar{X}_{\mathrm{L}}(k+q)\Psi_{\mathrm{L}}(k) - \bar{\Psi}_{\mathrm{L}}(k) X_{\mathrm{L}}(k-q)\right)\phi_{\mathrm{L}}(q) \\ &+ \frac{1}{2}\int_{\Lambda/b} \frac{d^D k}{(2\pi)^D} \delta_\phi k^2 \phi_{\mathrm{L}}(-k)\phi_{\mathrm{L}}(k) \\ &+ \frac{\lambda}{4!}\delta_\lambda \int_{\Lambda/b} \frac{d^D k d^D p d^D q}{(2\pi)^{3D}} \phi_{\mathrm{L}}(-k)\phi_{\mathrm{L}}(k+q)\phi_{\mathrm{L}}(-p-q)\phi_{\mathrm{L}}(p). \end{aligned} \tag{22}$$

Note that δ_Ψ, δ_X, δ_M, and δ_ϕ are obtained from self-energy corrections of each field, and δ_g and δ_λ are obtained from vertex corrections, and all δ_a, $a = \Psi, X, \phi, g, \lambda$ are functions of scaling parameter b. Including the corrections and rescaling of the momentum $k \mapsto k/b$, the renormalized action is

$$
\begin{aligned}
S_{\mathrm{R}} = S_{\mathrm{L}} + \delta S = \int_{\Lambda} \frac{d^D k}{(2\pi)^D}\, b^{-D-1} Z_{\Psi}^{-1} \bar{\Psi}_{\mathrm{L}}(k/b) \mathrm{i}\gamma \cdot k \Psi_{\mathrm{L}}(k/b) + \int_{\Lambda} \frac{d^D k}{(2\pi)^D}\, \bar{X}_{\mathrm{L}}(k/b)\, \mathrm{i}\gamma \\
\cdot (b^{-D-1} Z_X^{-1} k + b^{-D} Z_M^{-1} M) X_{\mathrm{L}}(k/b) \\
-\mathrm{i} g Z_g^{-1} b^{-2D} \int_{\Lambda} \frac{d^D k d^D q}{(2\pi)^{2D}}\, \big(\bar{X}_{\mathrm{L}}(k/b + q/b) \Psi_{\mathrm{L}}(k/b) - \bar{\Psi}_{\mathrm{L}}(k/b) X_{\mathrm{L}}(k/b - q/b)\big) \phi_{\mathrm{L}}(q/b) \\
+\frac{1}{2} \int_{\Lambda} \frac{d^D k}{(2\pi)^D}\, b^{-D-2} Z_{\phi}^{-1} k^2 \phi_{\mathrm{L}}(-k/b) \phi_{\mathrm{L}}(k/b) \\
+ \frac{\lambda}{4!} b^{-3D} Z_{\lambda}^{-1} \int_{\Lambda} \frac{d^D k d^D p d^D q}{(2\pi)^{3D}}\, \phi_{\mathrm{L}}(-k/b) \phi_{\mathrm{L}}(k/b + q/b) \phi_{\mathrm{L}}(-p/b \\
- q/b) \phi_{\mathrm{L}}(p/b),
\end{aligned}
\tag{23}
$$

where $Z_a^{-1} = 1 + \delta_a$, $a = \Psi, X, \phi, g, \lambda$. Concerning the free parts, we define renormalized fields as

$$
\Psi_{\mathrm{R}}(k) = b^{-\frac{D+1}{2}} Z_{\Psi}^{-\frac{1}{2}} \Psi_{\mathrm{L}}(k/b), X_{\mathrm{R}}(k) = b^{-\frac{D+1}{2}} Z_X^{-\frac{1}{2}} X_{\mathrm{L}}(k/b), \phi_{\mathrm{R}}(k) = b^{-\frac{D+2}{2}} Z_{\phi}^{-\frac{1}{2}} \phi_{\mathrm{L}}(k/b). \tag{24}
$$

Expressing the interactions in terms of renormalized fields, we obtain renormalized couplings,

$$
g_{\mathrm{R}} = b^{2-\frac{D}{2}} Z_g^{-1} Z_{\Psi}^{\frac{1}{2}} Z_X^{\frac{1}{2}} Z_{\phi}^{\frac{1}{2}} g, \lambda_{\mathrm{R}} = b^{4-D} Z_{\lambda}^{-1} Z_{\phi}^{2} \lambda, M_{\mathrm{R}} = b Z_M^{-1} Z_X M. \tag{25}
$$

Then the renormalized action becomes the same form as the original action, but now in terms of renormalized fields and couplings as

$$
\begin{aligned}
S_{\mathrm{R}} = \int_{\Lambda} \frac{d^D k}{(2\pi)^D}\, \bar{\Psi}_{\mathrm{R}}(k) \mathrm{i}\gamma \cdot k \Psi_{\mathrm{R}}(k) + \int_{\Lambda} \frac{d^D k}{(2\pi)^D}\, \bar{X}_{\mathrm{R}}(k) \mathrm{i}\gamma \cdot (k + M_{\mathrm{R}}) X_{\mathrm{R}}(k) \\
-\mathrm{i} g_{\mathrm{R}} \int_{\Lambda} \frac{d^D k d^D q}{(2\pi)^{2D}}\, \big(\bar{X}_{\mathrm{R}}(k+q) \Psi_{\mathrm{R}}(k) - \bar{\Psi}_{\mathrm{R}}(k) X_{\mathrm{R}}(k-q)\big) \phi_{\mathrm{R}}(q) \\
+\frac{1}{2} \int_{\Lambda} \frac{d^D k}{(2\pi)^D}\, k^2 \phi_{\mathrm{R}}(-k) \phi_{\mathrm{R}}(k) + \frac{\lambda_{\mathrm{R}}}{4!} \int_{\Lambda} \frac{d^D k d^D p d^D q}{(2\pi)^{3D}}\, \phi_{\mathrm{R}}(-k) \phi_{\mathrm{R}}(k+q) \phi_{\mathrm{R}}(-p-q) \phi_{\mathrm{R}}(p).
\end{aligned}
\tag{26}
$$

Now the 'integral' equations (25) become translated into differential equations as follows

$$
\begin{aligned}
\eta_{\Psi} = \frac{1}{2} \frac{d\log Z_{\Psi}}{d\log b}, \quad \eta_X = \frac{1}{2} \frac{d\log Z_X}{d\log b}, \quad \eta_{\phi} = \frac{1}{2} \frac{d\log Z_{\phi}}{d\log b}, \\
\beta_g \equiv \frac{d g_{\mathrm{R}}}{\mathrm{d}\log b} = g_{\mathrm{R}} \left(2 - \frac{D}{2} - \frac{\mathrm{d}\log Z_g}{\mathrm{d}\log b} + \eta_{\Psi} + \eta_X + \eta_{\phi}\right), \\
\beta_{\lambda} \equiv \frac{d\lambda_{\mathrm{R}}}{\mathrm{d}\log b} = \lambda_{\mathrm{R}} \left(4 - D - \frac{\mathrm{d}\log Z_{\lambda}}{\mathrm{d}\log b} + 4\eta_{\phi}\right).
\end{aligned}
\tag{27}
$$

Here, η_{Ψ}, η_X, and η_{ϕ} represent anomalous scaling dimensions of each field variable, which results from correlated dynamics near quantum criticality. β_g and β_{λ} describe how each interaction parameter evolves as a function of an energy scale b self-consistently due to correlation effects. The initial condition of the effective field theory at Λ is defined as $b = 1$ while $b \to \infty$ gives rise to the low energy renormalization.

The functional integration for high energy degrees of freedom contributes self-energy corrections to low energy degrees of freedom

$$
\Sigma_{\Psi}(k) = g^2 \int_{\frac{\Lambda}{b}}^{\Lambda} \frac{d^D q}{(2\pi)^D}\, G_X(k+q) G_{\phi}(q), \quad \Sigma_X(k) = g^2 \int_{\frac{\Lambda}{b}}^{\Lambda} \frac{d^D q}{(2\pi)^D}\, G_{\Psi}(k+q) G_{\phi}(q), \tag{28}
$$

$$\Sigma_{\phi,1}(q) = -2g^2 \int_{\frac{\Lambda}{b}}^{\Lambda} \frac{d^D k}{(2\pi)^D} \mathrm{Tr}\, G_\Psi(k+q) G_X(k), \quad \Sigma_{\phi,2}(q) = -\frac{\lambda}{2} \int_{\frac{\Lambda}{b}}^{\Lambda} \frac{d^D k}{(2\pi)^D} G_\phi(k),$$

as represented in the form of Feynman diagrams of Supplementary Figure 6. In this context, the three-point vertex with the coupling constant g contributes self-energy corrections to all excitations of $\Psi(k)$, $X(k)$, and $\phi(q)$ in the one-loop level. In addition, the self-interaction vertex with the coupling constant λ results in the self-energy correction on the Ising spin AFM fluctuations [19]. Green's functions are given by

$$G_\Psi(k) = -\frac{\mathrm{i}\gamma \cdot k}{k^2}, \qquad G_X(k) = -\frac{\mathrm{i}\gamma \cdot (k+M)}{(k+M)^2}, \qquad G_\phi(k) = \frac{1}{k^2 + r}. \tag{29}$$

The Ψ-propagator $G_\Psi(k)$, X-propagator $G_X(k)$, and ϕ-propagator $G_\phi(k)$ are represented by a single line, double line, and dashed line, respectively, as shown in Fig. S7. Hereafter, we focus on the zigzag AFM quantum criticality at $r = 0$.

Such quantum fluctuations also affect the vertices and contribute to corrections of

$$\Gamma_g = -\mathrm{i}g^3 \int_{\frac{\Lambda}{b}}^{\Lambda} \frac{d^D q}{(2\pi)^D} G_\phi(q) G_\Psi(q) G_X(q),$$

$$\Gamma_{\lambda,1} = -\frac{3\lambda^2}{2} \int_{\frac{\Lambda}{b}}^{\Lambda} \frac{d^D q}{(2\pi)^D} [G_\phi(q)]^2, \quad \Gamma_{\lambda,2} = g^4 \int_{\frac{\Lambda}{b}}^{\Lambda} \frac{d^D q}{(2\pi)^D} \mathrm{Tr}\, G_X(q) G_\Psi(q) G_X(q) G_\Psi(q). \tag{30}$$

See Supplementary Fiture 6 for Feynman diagrams. The three-point vertex is renormalized by itself in the one-loop level and also gives rise to the vertex renormalization for the four-point λ-vertex of the Ising spin fluctuations. The self-interaction vertex is also renormalized by itself in the one-loop level, and its renormalization typically leads to the Wilson-Fisher fixed point [16]. Here, we only consider the most relevant interaction channels with zero energy-momentum transfer.

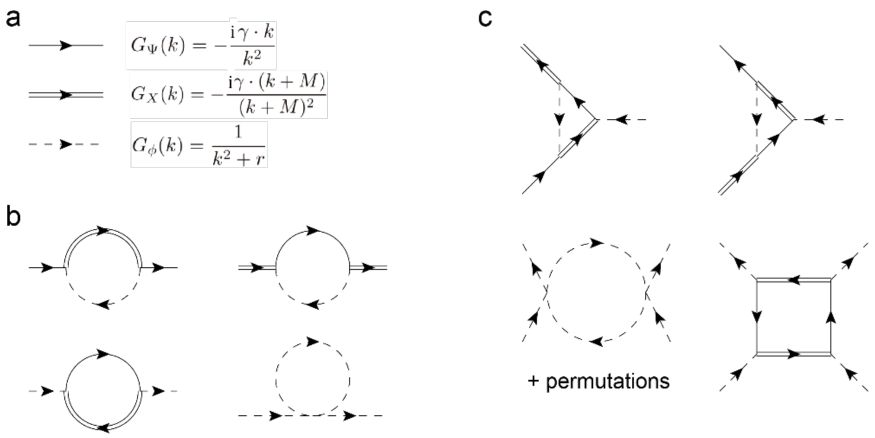

Supplementary Figure 6. Feynman diagrams for self-energies and vertex corrections. a The solid line, double line, and dashed line represent the Ψ propagator $G_\Psi(k)$, X propagator $G_X(k)$, and ϕ propagator $G_\phi(k)$, respectively. **b** The three-point interaction vertex with g contributes self-energy corrections to all excitations of $\Psi(k)$, $X(k)$, and $\phi(q)$ in the one-loop level. In addition, the self-interaction vertex with λ causes the mass renormalization, but does not the wave-function renormalization in the one-loop level. **c** The three-point (four-point or self-interaction) vertex becomes renormalized by itself and additionally gives rise to the four-point vertex renormalization in the one-loop level.

In the end of this Supplementary Notes(Calculation details), we describe all details of integrals for both self-energy and vertex corrections. Here we present all renormalization constants as follows

$$Z_\Psi = 1 - \frac{g_R^2}{2} S_D F_D^\Psi(M) \frac{dl}{\Lambda^{4-D}}, \quad Z_X = 1 - \frac{g_R^2}{2} S_D \frac{dl}{\Lambda^{4-D}}, \quad Z_\phi = 1 - g_R^2 S_D F_D^\phi(M) \frac{dl}{\Lambda^{4-D}},$$
$$Z_g = 1 + g_R^2 S_D G_D^g(M) \frac{dl}{\Lambda^{4-D}}, \quad Z_\lambda = 1 + \frac{3\lambda_R}{2} S_D \frac{dl}{\Lambda^{4-D}} - 12 \frac{g_R^4}{\lambda_R} S_D G_D^\lambda(M) \frac{dl}{\Lambda^{4-D}}, \text{ and} \tag{31}$$
$$Z_M = 1 + \frac{g_R^2}{2} S_D G_D^M(M) \frac{dl}{\Lambda^{4-D}},$$

where $S_D = \frac{2\pi^{D/2}}{(2\pi)^D \Gamma(D/2)}$ is the surface area of the D-dimensional sphere, and the high energy-momentum domain is $dl = \log b$. The wave-function renormalization constant Z_ϕ for the zigzag spin-fluctuation field $\phi(k)$ originates from the three-point interaction vertex rather than the four-point self-interaction vertex in the one-loop level. Both three-point and four-point interaction vertices contribute to the four-point vertex renormalization constant in the one-loop level.

The mass-dependent functions, $F_D^{\Psi,\phi}(M)$ and $G_D^{g,\lambda,M}(M)$ in the renormalization constants are as follows

$$F_D^\Psi(M) = \frac{2}{\sqrt{\pi}} \frac{\Gamma\left(\frac{D}{2}\right)}{\Gamma\left(\frac{D-1}{2}\right)} \int_0^1 ds \int_0^\pi d\phi \, \frac{(1-s)\sin^{D-2}\phi}{\left(1 + \frac{sM^2}{\Lambda^2} + \frac{2sM}{\Lambda}\cos\phi\right)^2},$$

$$F_D^\phi(M)$$
$$= \frac{2}{\sqrt{\pi}} \frac{\Gamma\left(\frac{D}{2}\right)}{\Gamma\left(\frac{D-1}{2}\right)} \int_0^1 ds \int_0^\pi d\phi \, \sin^{D-2}\phi \frac{3s(1-s) + s^2(1-s)\frac{M^2}{\Lambda^2} + 2s(1-s^2)\frac{M}{\Lambda}\cos\phi}{\left(1 + \frac{sM^2}{\Lambda^2} + \frac{2sM}{\Lambda}\cos\phi\right)^2},$$

$$G_D^g(M) = \frac{2}{\sqrt{\pi}} \frac{\Gamma\left(\frac{D}{2}\right)}{\Gamma\left(\frac{D-1}{2}\right)} \int_0^1 ds \int_0^\pi d\phi \, \frac{(1-s)\sin^{D-2}\phi\left(1 + \frac{M}{\Lambda}\cos\phi\right)}{\left(1 + \frac{sM^2}{\Lambda^2} + \frac{2sM}{\Lambda}\cos\phi\right)^3}, \tag{32}$$

$$G_D^\lambda(M) = \frac{2}{\sqrt{\pi}} \frac{\Gamma\left(\frac{D}{2}\right)}{\Gamma\left(\frac{D-1}{2}\right)} \int_0^1 ds \int_0^\pi d\phi \, s(1-s)\sin^{D-2}\phi \frac{1 + \frac{2M}{\Lambda}\cos\phi + \frac{2M^2}{\Lambda^2}\cos^2\phi - \frac{M^2}{\Lambda^2}}{\left(1 + \frac{sM^2}{\Lambda^2} + \frac{2sM}{\Lambda}\cos\phi\right)^4}, \text{and}$$

$$G_D^M(M) = \frac{2}{\sqrt{\pi}} \frac{\Gamma\left(\frac{D}{2}\right)}{\Gamma\left(\frac{D-1}{2}\right)} \int_0^1 ds \int_0^\pi d\phi \, \frac{\sin^{D-2}\phi}{\left(1 + \frac{sM^2}{\Lambda^2} + \frac{2sM}{\Lambda}\cos\phi\right)^2}.$$

$F_D^\Psi(M)$ ($F_D^\phi(M)$) results from the self-energy correction for Ψ spinons (ϕ Ising spin fluctuations). $G_D^g(M)$ and $G_D^\lambda(M)$ come from quantum corrections for the three-point vertex with g and the self-interaction vertex with λ, respectively. Self-energies of the Ψ and X fields cause mass renormalization $G_D^M(M)$, which expands the difference between zero energy momentum points (the so-called Dirac points) of the Ψ and X fields.

Inserting the renormalization constants in Eq. (31) into Eq. (27), we derive the anomalous scaling dimensions

$$\eta_\Psi = \frac{1}{2}\frac{d\log Z_\Psi}{dl} = -\frac{g^2}{32\pi^2} F_4^\Psi(M), \ \eta_X = \frac{1}{2}\frac{d\log Z_X}{dl} = -\frac{g^2}{32\pi^2},$$
$$\eta_\phi = \frac{1}{2}\frac{d\log Z_\phi}{dl} = -\frac{g^2}{16\pi^2} F_4^\phi(M), \tag{33}$$

and the β-functions

$$\beta_g = \frac{g}{2} - \frac{g^3}{16\pi^2}\left(2G_4^g(M) + \frac{1}{2}F_4^\Psi(M) + F_4^\phi(M) + \frac{1}{2}\right), \ \beta_\lambda = \lambda - \frac{3\lambda^2}{16\pi^2} + \frac{3g^4}{2\pi^2} G_4^\lambda(M). \tag{34}$$

Here we consider $D = 4 - \epsilon$ with $\epsilon = 1$ and obtain the mass-dependent functions as follows

$$
\begin{aligned}
F_4^{\Psi}(M) &= \frac{4}{\pi}\int_0^1 ds \int_0^{\pi} d\phi\, \sin^2\phi \frac{1-s}{(1+sM^2+2sM\cos\phi)^2},\\
F_4^{\phi}(M) &= \frac{4}{\pi}\int_0^1 ds \int_0^{\pi} d\phi\, \sin^2\phi \frac{3s(1-s)+s^2(1-s)M^2+2s(1-s^2)M\cos\phi}{(1+sM^2+2sM\cos\phi)^3},\\
G_4^{g}(M) &= \frac{4}{\pi}\int_0^1 ds \int_0^{\pi} d\phi\, \sin^2\phi \frac{(1-s)(1+2M\cos\phi)}{(1+sM^2+2sM\cos\phi)^3},\\
G_4^{\lambda}(M) &= \frac{4}{\pi}\int_0^1 ds \int_0^{\pi} d\phi\, s(1-s)\sin^2\phi \frac{1+\frac{2M}{\Lambda}\cos\phi+\frac{2M^2}{\Lambda^2}\cos^2\phi-\frac{M^2}{\Lambda^2}}{\left(1+\frac{sM^2}{\Lambda^2}+\frac{2sM}{\Lambda}\cos\phi\right)^4}.
\end{aligned}
\tag{35}
$$

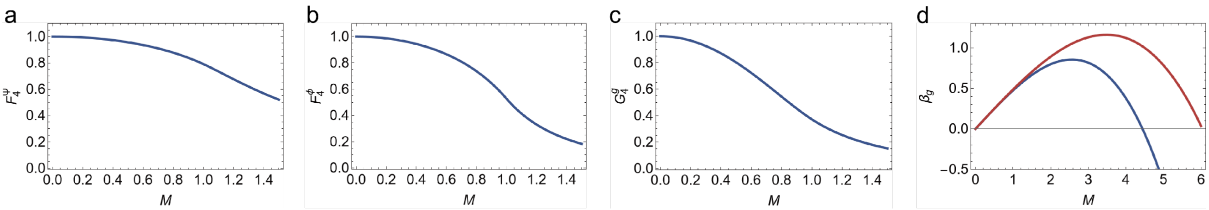

Supplementary Figure 7. The functions $F_4^{\Psi}(M)$, $F_4^{\phi}(M)$, $G_4^{g}(M)$ and the β-function β_g. We plot **a** $F_4^{\Psi}(M)$, **b** $F_4^{\phi}(M)$, and **c** $G_4^{g}(M)$ as a function of M, respectively. **d** β_g in terms of g with $M = 0$ (blue) and $M = 1$ (red).

It is straightforward to solve the coupled β-functions (34), and the interaction parameter g between spinon excitations and Ising spin fluctuations evolves to decouple from the self-interaction constant λ. The fixed point for the three-point interaction vertex is given by

$$
\frac{g_*^2}{8\pi^2} = \left(2G_4^{g}(M) + \frac{F_4^{\Psi}(M)}{2} + F_4^{\phi}(M) + \frac{1}{2}\right)^{-1}. \tag{36}
$$

This interacting fixed point is stable, as expected for the three-point interaction vertex in the abelian case. However, this effective interaction causes instability on the Wilson-Fisher fixed point, leading to a interacting fixed point

$$
\lambda_* = \frac{\lambda_{WF} + \sqrt{\lambda_{WF}^2 + 32 g_*^4 G_4^{\lambda}(M)}}{2}, \tag{37}
$$

where $\lambda_{WF} = 16\pi^2/3$ is the Wilson-Fisher fixed point. Supplementary Figure 5 displays the flow diagram of the β-functions together with the new fixed point.

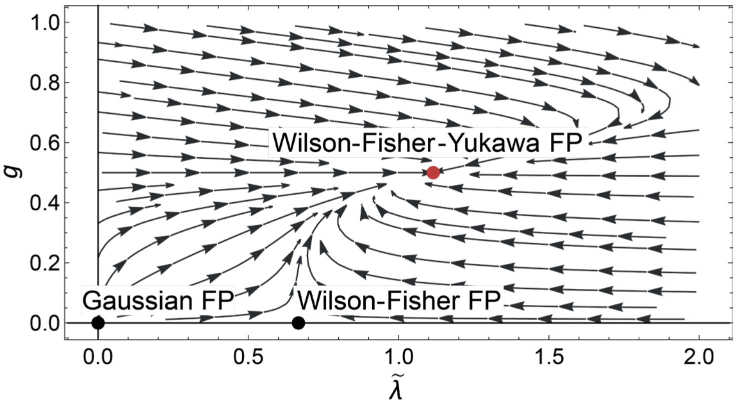

Supplementary Figure 8. The renormalization group flow diagram of coupling constants. Solving the coupled β-functions, we find RG flows in a $\tilde{g}-\tilde{\lambda}$ coupling space with $\tilde{g}^2 = g^2/8\pi^2$ and $\tilde{\lambda} = \lambda/8\pi^2$, and obtain a novel interacting fixed point.

Inserting this fixed-point value into Eq. (33), we have

$$\begin{aligned}
\eta_\Psi &= -\frac{F_4^\Psi(M)}{4\left(2G_4^g(M) + \frac{F_4^\Psi(M)}{2} + F_4^\phi(M) + \frac{1}{2}\right)}, \\
\eta_X &= -\frac{1}{4\left(2G_4^g(M) + \frac{F_4^\Psi(M)}{2} + F_4^\phi(M) + \frac{1}{2}\right)}, \qquad (38) \\
\eta_\phi &= -\frac{F_4^\phi(M)}{2\left(2G_4^g(M) + \frac{F_4^\Psi(M)}{2} + F_4^\phi(M) + \frac{1}{2}\right)}.
\end{aligned}$$

It is interesting to observe that the Ising spin field $\phi(k)$ acquires an anomalous scaling dimension in the one-loop level through interactions with spinon excitations. Meanwhile, without the three-point vertex, the anomalous scaling dimension requires the two-loop order at the Wilson-Fisher fixed point.

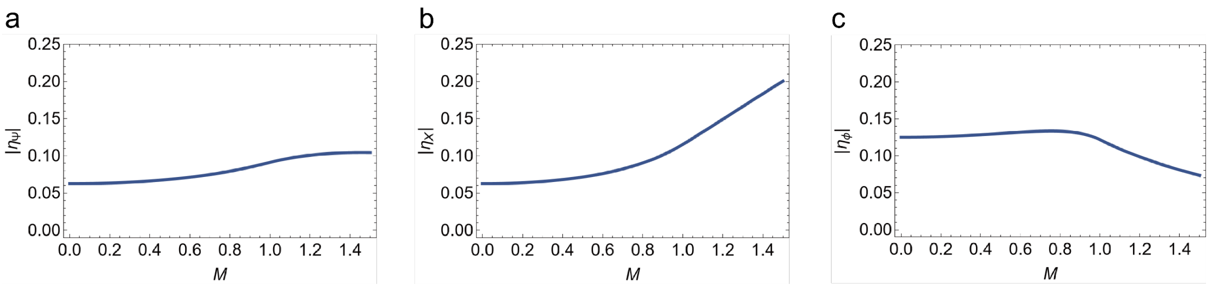

Supplementary Figure 9. Anomalous scaling dimensions. Anomalous scaling dimensions as a function of the Z_2 flux gap M for **a** η_Ψ, **b** η_X, and **c** η_ϕ.

3. Dynamic spin susceptibility

In order to extract the dynamical spin susceptibility at the Γ-point, we introduce a uniform field Zeeman coupling $H_{\mathrm{UZ}} = -g_u \sum_i \sigma_i^z H_i^u$, which can be reformulated as

$$H_{\mathrm{UZ}} = \mathrm{i}g_{\mathrm{u}} \int \frac{d^3k d^3q}{(2\pi)^6} H_u(q)\big(\bar{X}(k+q)\gamma_0\Psi(k) - \bar{\Psi}(k)\gamma_0 X(k-q)\big). \tag{39}$$

Here, we do not take into account for the coupling between the zigzag AFM $\phi(k)$ and the uniform field since its effect is negligible in comparison with the ferro-component contribution of the Γ-point. Then, the spin susceptibility is given by

$$\chi_{\mathrm{u}}(q) = \frac{1}{V}\frac{\delta^2 \ln Z_{\mathrm{eff}}[H(q)]}{\delta H_u(-q)\delta H_u(q)}\bigg|_{H(q)=0}, \tag{40}$$

where Z_{eff} is the effective partition function including the Zeeman term. This 2nd derivative of the effective free energy with resect to the magnetic field reduces to the Kubo formula for the spin susceptibility as like

$$\begin{aligned}\chi_{\mathrm{u}}(q) &= g_{\mathrm{u}}^2 Z_{g_{\mathrm{u}}}^2 Z_\Psi Z_X \frac{1}{V}\int_{k,k'} (\langle \bar{X}_{\mathrm{R}}(k+q)\gamma_0\Psi_{\mathrm{R}}(k)\bar{\Psi}_{\mathrm{R}}(k')\gamma_0 X_{\mathrm{R}}(k'+q)\rangle_{\mathrm{c}} \\ &\quad + \langle \bar{\Psi}_{\mathrm{R}}(k)\gamma_0 X_{\mathrm{R}}(k-q)\bar{X}_{\mathrm{R}}(k'-q)\gamma_0\Psi_{\mathrm{R}}(k')\rangle_{\mathrm{c}}) \\ &= -g_{\mathrm{u}}^2 Z_{g_{\mathrm{u}}}^2 Z_\Psi Z_X \int_k \mathrm{Tr}\,[\{G_X(k+q) + G_X(k-q)\}\gamma_0 G_\Psi(k)\gamma_0] \equiv g_{\mathrm{u}}^2 Z_{g_{\mathrm{u}}}^2 Z_\Psi Z_X \chi_{\mathrm{R}}(q),\end{aligned} \tag{41}$$

where $Z_{g_{\mathrm{u}}}$ is the renormalization constant for the effective coupling constant in the Zeeman term. The renormalization factors play roles of anomalous scaling dimensions in the spin susceptibility and account for the absence of well defined quasiparticle excitations near the interacting fixed point.

Inserting the spinon Green's functions into the above expression, we obtain $\chi_{\mathrm{R}}(q) \equiv \chi_\Gamma^{(0)}(\mathrm{i}\nu, q)$ at finite temperatures,

$$\chi_\Gamma^{(0)}(\mathrm{i}\nu, q) = -\frac{g_{\mathrm{u}}^2}{\beta}\sum_{\mathrm{i}\omega}\int \frac{d^2k}{(2\pi)^2}\,\mathrm{Tr}\left[\frac{-\mathrm{i}\gamma_0(\omega+\nu) - \mathrm{i}\vec{\gamma}\cdot(\vec{k}+\vec{q}+\vec{M})}{(\omega+\nu)^2 + (\vec{k}+\vec{q}+\vec{M})^2}\gamma_0 \frac{-\mathrm{i}\gamma_0\omega - \mathrm{i}\gamma\cdot k}{\omega^2 + k^2}\gamma_0\right] + (q \to -q). \tag{42}$$

After detailed calculations presented in the end of the Supplementary Note (Calculation details), we obtain $\chi_\Gamma^{(0)}(\mathrm{i}\nu, q)$ in a BCS (Bardeen-Cooper-Schrieffer) form with a coherence factor. Taking the analytic continuation for the frequency $\mathrm{i}\nu \to \nu + \mathrm{i}\delta$, we finally determine the imaginary part of the spin susceptibility $\chi_{\mathrm{u}}(q) \equiv \chi_\Gamma(\mathrm{i}\nu, q)$ at the Γ point ($\vec{q} \to 0$) as follows,

$$\mathrm{Im}\chi_\Gamma(\nu, q\to 0) = Z_{g_{\mathrm{u}}}^2 Z_\Psi Z_X \begin{cases} \dfrac{g_{\mathrm{u}}^2}{2\pi}\displaystyle\int_0^\pi d\theta\, k_0 \frac{\nu - 2k_0 - M\cos\theta}{\nu + M\cos\theta}\left(\tanh\frac{k_0}{2T} - \tanh\frac{k_0-\nu}{2T}\right) & (\nu > M) \\ \dfrac{g_{\mathrm{u}}^2}{2\pi}\displaystyle\int_{\pi-\theta_1}^\pi d\theta\, k_1 \frac{\nu + 2k_1 + M\cos\theta}{\nu - M\cos\theta}\left(\tanh\frac{k_1+\nu}{2T} - \tanh\frac{k_1}{2T}\right) & \\ + \dfrac{g_{\mathrm{u}}^2}{2\pi}\displaystyle\int_{\pi-\theta_2}^\pi d\theta\, k_2 \frac{\nu - 2k_2 - M\cos\theta}{\nu + M\cos\theta}\left(\tanh\frac{k_2}{2T} - \tanh\frac{k_2-\nu}{2T}\right) & (\nu < M) \end{cases} \tag{43}$$

where we used short-hand notations

$$k_0 = \frac{1}{2}\frac{\nu^2 - M^2}{\nu + M\cos\theta}, \qquad k_1 = \frac{1}{2}\frac{M^2 - \nu^2}{\nu - M\cos\theta}, \qquad k_2 = \frac{1}{2}\frac{\nu^2 - M^2}{\nu + M\cos\theta} = k_0,$$
$$\cos\theta_1 = \frac{\nu}{M}, \qquad \cos\theta_2 = -\frac{\nu}{M}. \tag{44}$$

In order to introduce anomalous scaling dimensions, we rewrite the renormalization constants as

$$Z_\Psi = 1 - \frac{g_{\mathrm{R}}^2 S_D}{2\Lambda^{4-D}} F_D^\Psi(M) \ln b \approx \mathrm{e}^{-\frac{g_{\mathrm{R}}^2 S_D}{2\Lambda^{4-D}} F_D^\Psi(M) \ln b} = b^{2\eta_\Psi},$$
$$Z_X = 1 - \frac{g_{\mathrm{R}}^2 S_D}{2\Lambda^{4-D}} \ln b \approx \mathrm{e}^{-\frac{g_{\mathrm{R}}^2 S_D}{2\Lambda^{4-D}} \ln b} = b^{2\eta_X}. \tag{45}$$

Here, we do not take into account the anomalous scaling of g_{u}, given by $Z_{g_{\mathrm{u}}}$ at the leading order. Then, we find the scaling theory for the spin susceptibility

$$\mathrm{Im}\chi(\nu, M, T) = s^{1+2\eta_\Psi+2\eta_X} \mathrm{Im}\chi\left(\frac{\nu}{s}, \frac{M}{s^{y_M}}, \frac{T}{s}\right) = T^{1+2\eta_\Psi+2\eta_X} \mathrm{Im}\chi\left(\frac{\nu}{T}, \frac{M}{T^{y_M}}, 1\right), \tag{46}$$

where we set $s = T$ in the second equality and y_M is the scaling dimension of M. Assuming $M/T^{y_M} \ll 1$, we can expand $\chi(\nu/T, M/T^{y_M}, 1)$ in M/T^{y_M}. Based on Eq. (43), we find that the lowest non-vanishing term is $(M/T^{y_M})^2$. Accordingly, the spin susceptibility is given by

$$\mathrm{Im}\chi(\nu, M, T) = \chi_0 T^{1+2\eta_\Psi+2\eta_X} (M/T^{y_M})^2 \left(\frac{T}{\nu}\right)^{1-2\eta_\Psi-2\eta_X} \tanh\frac{\nu}{4T} \equiv T^{-\eta_\chi} f\left(\frac{\nu}{T}\right), \tag{47}$$

where χ_0 is a cut-off dependent and non-universal constant. The anomalous scaling dimension of the spin susceptibility is $\eta_\chi = 2y_M - (1 + 2\eta_\Psi + 2\eta_X)$ and the scaling function is $f\left(\frac{\nu}{T}\right) = \chi_0 M^2 \left(\frac{T}{\nu}\right)^{1-2\eta_\Psi-2\eta_X} \tanh\frac{\nu}{4T}$.

B. Effective field theory, dynamic spin susceptibility, specific heat, and dynamical mean-field theory analysis for the low-energy strong-coupling fixed point

1. Effective field theory, dynamic spin susceptibility, and specific heat for the local quantum criticality

We start from an empirical formula for the spin susceptibility with an external magnetic field H [20]

$$\chi_{\mathrm{LQCP}}(\omega, T, H) = \frac{A}{(aT - \mathrm{i}\omega)^\alpha + a^\alpha T_{\mathrm{N}}^\alpha}, \qquad T_{\mathrm{N}} = T_{\mathrm{N}}(H = 0)\delta h^{\nu z}. \tag{48}$$

Here, ω and T are frequency and temperature, respectively. T_{N} is the Néel temperature, and $\delta h = 1 - H/H_{\mathrm{C}}$, where H_{C} is the critical field. The exponent $\nu z \approx 0.125$ is experimentally determined from the specific heat data shown in Fig. 8b in the main text. Parameters A, a, and α can be obtained from fitting of the spin susceptibility data. The explicit form used in the fitting is the imaginary part of χ_{LQCP} at the critical field, $H = H_{\mathrm{C}}$ so $T_{\mathrm{N}} = 0$;

$$\mathrm{Im}\chi_{\mathrm{LQCP}}(\omega, T, H_{\mathrm{C}}) = \mathrm{Im}\frac{A}{(aT - \mathrm{i}\omega)^\alpha} = T^{-\alpha} \frac{A}{(a^2T^2 + \omega^2)^{\alpha/2}} \sin\left(\alpha \tan^{-1}\frac{\omega}{aT}\right), \tag{49}$$

which is Eq. (2) in the main text.

Based on this local form of the spin susceptibility, we write an effective action for the low-energy region as

$$Z = \int D\psi D\chi D\phi \ \mathrm{e}^{-S[\psi,\chi,\phi]},$$
$$\begin{aligned} S[\psi,\chi,\phi] = \int_0^\beta d\tau \int d^2x \ \Big[&\bar\psi(\tau,x)\big(\gamma^\tau\partial_\tau + v_\psi\gamma^i\partial_i\big)\psi(\tau,x) + \bar\chi(\tau,x)\big(\gamma^\tau\partial_\tau + \mathrm{i}\gamma^i M_i\big)\psi(\tau,x) \\ &- \mathrm{i}\lambda\phi(\tau,x)\left(\bar\chi(\tau,x)\psi(\tau,x) - \bar\psi(\tau,x)\chi(\tau,x)\right)\Big] \\ &+ \frac{1}{2}\int_0^\beta d\tau\, d\tau' \int d^2x \ \phi(\tau,x)\chi_{\mathrm{LQCP}}^{-1}(\tau-\tau')\phi(\tau',x). \end{aligned} \tag{50}$$

This expression looks quite similar to that for the description of high energy delocalized quantum criticality. However, there exist two essential different aspects. Firstly, the spin dynamics is locally critical, described by $\chi_{\mathrm{LQCP}}^{-1}$ in the AFM spin-fluctuation part instead of the relativistic dispersion. In the Matsubara frequency space, $\chi_{\mathrm{LQCP}}^{-1}$ has the following form [19]

$$\chi_{\mathrm{LQCP}}^{-1}(\mathrm{i}\omega, T, H) = [(aT + |\omega|)^{\alpha} + a^{\alpha} T_{\mathrm{N}}^{\alpha}]/A \tag{51}$$

assumed to be momentum independent based on both spectroscopy and specific heat results (experiments) as shown in the main text. Secondly, the dynamics of Z_2 flux excitations is also local. Below, we perform the dynamical mean-field theory analysis in the non-crossing approximation [21, 22], which confirms that this renormalization ansatz is self-consistent.

Integrating over the ϕ-field, we obtain the following effective action

$$Z = \int D\psi D\chi \ \mathrm{e}^{-S[\psi,\chi]},$$

$$\begin{aligned} S[\psi,\chi] = {} & \frac{1}{2}\mathrm{Tr}\log \chi_{\mathrm{LQCP}}^{-1} \\ & + \int_0^{\beta} d\tau \int d^2x \ \left[\bar{\psi}(\tau,x)\left(\gamma^{\tau}\partial_{\tau} + v_{\psi}\gamma^{i}\partial_{i}\right)\psi(\tau,x) + \bar{\chi}(\tau,x)(\gamma^{\tau}\partial_{\tau} + \mathrm{i}\gamma^{i}M_{i})\psi(\tau,x)\right] \\ & - \frac{\lambda^2}{2}\int_0^{\beta} d\tau\, d\tau' \int d^2x \,[\bar{\chi}(\tau,x)\psi(\tau,x)\chi_{\mathrm{LQCP}}(\tau-\tau')\chi(\tau',x)\bar{\psi}(\tau',x) \\ & + \bar{\psi}(\tau,x)\chi(\tau,x)\chi_{\mathrm{LQCP}}(\tau-\tau')\psi(\tau',x)\bar{\chi}(\tau',x)]. \end{aligned} \tag{52}$$

Performing the self-consistent one-loop analysis in this effective field theory, we find that this effective field theory yields a fixed point, which is locally quantum critical, as a self-consistent solution. Here the pairing channel has been neglected for simplicity.

Based on this effective field theory, we calculate the free-energy

$$F = \frac{1}{2\beta}\mathrm{Tr}\log \chi_{\mathrm{LQCP}}^{-1}. \tag{53}$$

Here we neglect contributions of both fermions ψ and χ since excitations at low temperatures are dominated by the AFM critical bosons. It is because the Z_2 flux excitations are 'gapped' and the itinerant Majorana fermions have the Dirac dispersion. Now the specific heat is

$$C_{\mathrm{m}}(T) = -T\frac{\partial^2 F}{\partial T^2} = -\frac{T}{2\pi}\int_0^{\infty} dE \ \frac{\partial^2}{\partial T^2}\left(\coth\frac{E}{2T}\ \mathrm{Im}\log \chi_{\mathrm{LQCP}}^{-1}\right), \tag{54}$$

where

$$\mathrm{Im}\log \chi_{\mathrm{LQCP}}^{-1} = -\tan^{-1}\frac{(a^2+x^2)^{\frac{\alpha}{2}}\sin\alpha\theta}{(a^2+x^2)^{\frac{\alpha}{2}}\cos\alpha\theta + a^{\alpha}y^{\alpha}}, \qquad x = \frac{E}{T}, \qquad y = \frac{T_{\mathrm{N}}}{T}, \tag{55}$$

and $\theta = \tan^{-1}\frac{E}{aT}$. From this analytic form, one can deduce Eq. (54) as a function of T_{N}/T, or $\delta h^{vz}/T$. This scaling behavior originates from the local behavior of χ_{LQCP}. Using the values $\alpha \approx 0.14$ and $a \approx 0.88$ obtained from fitting the dynamic spin susceptibility (Fig. 6 in the main text), the calculated specific heat is shown in Supplementary Figure 10.

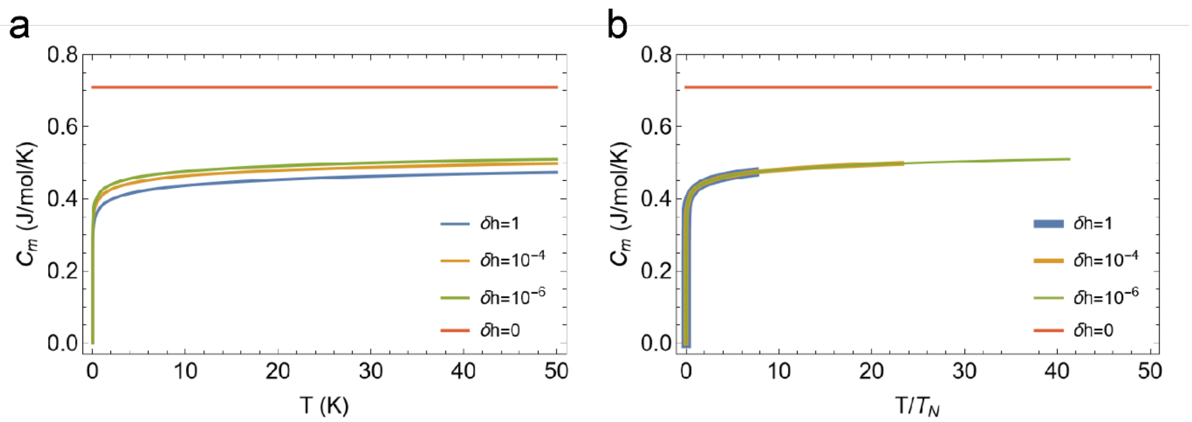

Supplementary Figure 10. Cacluated specific heat. a Specific heat C_{m} versus temperature T with various δh. **b** Scaling behavior of C_{m}. All curves with different δh collapse into a single curve. The value for the critical point ($\delta h = 0$) corresponds to the value at $T \to \infty$.

Note that the parameter $\alpha \approx 0.14$ is much smaller than $\alpha = 1$ for the dynamics of a decoupled local moment. This critical exponent of the spin susceptibility could explain the plateau behavior of the specific heat in the intermediate temperature regime as shown in the main text. We show that this small value is supported by the self-consistent one-loop calculation in the next section. We also point out that the slow convergence to the critical value is due to the small value of $\nu z \approx 0.125$, which is not well understood within the first principle.

2. Dynamical mean-field theory analysis for the low-energy strong-coupling fixed point

One-loop self-energies for both ψ and χ fermions are

$$\Sigma_\psi(\mathrm{i}\omega, \mathbf{k}) = -\frac{\lambda^2}{2\beta}\sum_{\mathrm{i}\Omega}\int \frac{d^d q}{(2\pi)^d}\, \chi_{\mathrm{LQCP}}(\mathrm{i}\Omega)\mathcal{g}_\chi(\mathrm{i}\omega - \mathrm{i}\Omega, \mathbf{k} - \mathbf{q}), \tag{56}$$

$$\Sigma_\chi(\mathrm{i}\omega, \mathbf{k}) = -\frac{\lambda^2}{2\beta}\sum_{\mathrm{i}\Omega}\int \frac{d^d q}{(2\pi)^d}\, \chi_{\mathrm{LQCP}}(\mathrm{i}\Omega)\mathcal{g}_\psi(\mathrm{i}\omega - \mathrm{i}\Omega, \mathbf{k} - \mathbf{q}), \tag{57}$$

where $\mathcal{g}_\psi(\mathrm{i}\omega, \mathbf{k})$ and $\mathcal{g}_\chi(\mathrm{i}\omega, \mathbf{k})$ are renormalized Green's functions of the ψ- and χ-fields. These renormalized Green's functions satisfy the Dyson equations as follows

$$\mathcal{g}_\psi^{-1}(\mathrm{i}\omega, \mathbf{k}) = \mathcal{g}_\psi^{(0)-1}(\mathrm{i}\omega, \mathbf{k}) - \Sigma_\psi(\mathrm{i}\omega, \mathbf{k}) = \gamma^\tau\left(\mathrm{i}\omega - \Sigma_{\psi,r}(\mathrm{i}\omega, \mathbf{k})\right) + \gamma^i\left(\mathrm{i}v_\psi k_i - \Sigma_{\psi,i}(\mathrm{i}\omega, \mathbf{k})\right), \tag{58}$$

$$\mathcal{g}_\chi^{-1}(\mathrm{i}\omega, \mathbf{k}) = \mathcal{g}_\chi^{(0)-1}(\mathrm{i}\omega, \mathbf{k}) - \Sigma_\chi(\mathrm{i}\omega, \mathbf{k}) = \gamma^\tau\left(\mathrm{i}\omega - \Sigma_{\chi,r}(\mathrm{i}\omega, \mathbf{k})\right) + \gamma^i\left(\mathrm{i}M_i - \Sigma_{\chi,i}(\mathrm{i}\omega, \mathbf{k})\right). \tag{59}$$

Here, $\mathcal{g}_\psi^{(0)}(\mathrm{i}\omega, \mathbf{k}) = \left[\gamma^\tau(\mathrm{i}\omega) + \gamma^i\left(\mathrm{i}v_\psi k_i\right)\right]^{-1}$ ($\mathcal{g}_\chi^{(0)}(\mathrm{i}\omega, \mathbf{k}) = [\gamma^\tau(\mathrm{i}\omega) + \gamma^i(\mathrm{i}M_i)]^{-1}$) is the bare Green's function for the ψ (χ) fermion field. $\Sigma_{\psi(\chi),\tau}(\mathrm{i}\omega, \mathbf{k})$ and $\Sigma_{\psi(\chi),i}(\mathrm{i}\omega, \mathbf{k})$ are the temporal and spatial components of $\Sigma_{\psi(\chi)}(\mathrm{i}\omega, \mathbf{k})$, respectively.

The last self-consistent condition is derived from the renormalized spin susceptibility. The spin susceptibility calculated with the renormalized Green's functions should be the same as $\chi_{\mathrm{LQCP}}(\mathrm{i}\omega)$ from which we have started. Thus, the self-consistent condition is

$$\chi_{\mathrm{LQCP}}(\mathrm{i}\omega) = \frac{1}{\beta}\sum_{\mathrm{i}\omega'}\int \frac{d^d k}{(2\pi)^d}\, \mathrm{Tr}\ \mathcal{g}_\chi(\mathrm{i}\omega', \mathbf{k})\mathcal{g}_\psi(\mathrm{i}\omega' + \mathrm{i}\omega, \mathbf{k} + \mathbf{q}). \tag{60}$$

Now we solve self-consistent equations formed by Eqs. (56), (57), and (60). As discussed in the main text, we consider the power-law ansatz in frequency for the self-energy corrections,

$$\Sigma_\psi(\mathrm{i}\omega,\mathbf{k}) = \Sigma_\psi(\mathrm{i}\omega) = C_\psi|\omega|^{\alpha_\psi}, \qquad \Sigma_\chi(\mathrm{i}\omega,\mathbf{k}) = \Sigma_\chi(\mathrm{i}\omega) = C_\chi|\omega|^{\alpha_\chi}. \tag{61}$$

Inserting these expressions into Eqs. (56) and (57) with the Dyson equations and the local spin susceptibility ansatz, we obtain

$$\gamma^\tau\Sigma_{\psi,\tau}(\mathrm{i}\omega) + \gamma^i\Sigma_{\psi,i}(\mathrm{i}\omega) = -\frac{\lambda^2}{2\beta}\sum_{\mathrm{i}\Omega}\int\frac{d^dq}{(2\pi)^d}\left[\frac{\chi_0}{(aT-\mathrm{i}\Omega)^\alpha}\frac{\gamma^\tau\left(\mathrm{i}\omega-\mathrm{i}\Omega-\Sigma_{\chi,\tau}\right)-\gamma^i\Sigma_{\chi,i}}{\left(\mathrm{i}\omega-\mathrm{i}\Omega-\Sigma_{\chi,\tau}\right)^2+{\Sigma_{\chi,i}}^2}\right]_{\mathrm{i}\omega-\mathrm{i}\Omega}, \tag{62}$$

$$\begin{aligned}&\gamma^\tau\Sigma_{\chi,\tau}(\mathrm{i}\omega) + \gamma^i\Sigma_{\chi,i}(\mathrm{i}\omega)\\ &= -\frac{\lambda^2}{2\beta}\sum_{\mathrm{i}\Omega}\int\frac{d^dq}{(2\pi)^d}\left[\frac{\chi_0}{(aT-\mathrm{i}\Omega)^\alpha}\frac{\gamma^\tau\left(\mathrm{i}\omega-\mathrm{i}\Omega-\Sigma_{\psi,\tau}\right)-\gamma^i\left(\mathrm{i}v_\psi(k_i-q_i)-\Sigma_{\psi,i}\right)}{\left(\mathrm{i}\omega-\mathrm{i}\Omega-\Sigma_{\psi,\tau}\right)^2+\left(\mathrm{i}v_\psi(k_i-q_i)-\Sigma_{\psi,i}\right)^2}\right]_{\mathrm{i}\omega-\mathrm{i}\Omega}.\end{aligned} \tag{63}$$

Perfoming the momentum integral in the second equation, we have

$$\Sigma_{\psi,\tau}(\mathrm{i}\omega) = -\frac{\lambda^2}{2\beta}\sum_{\mathrm{i}\Omega}\frac{\chi_0}{(aT-\mathrm{i}\Omega)^\alpha}\frac{1}{\mathrm{i}\omega-\mathrm{i}\Omega-\Sigma_{\chi,\tau}(\mathrm{i}\omega-\mathrm{i}\Omega)}, \qquad \Sigma_{\psi,i} = 0, \tag{64}$$

$$\begin{aligned}\Sigma_{\chi,\tau}(\mathrm{i}\omega) &= -\frac{\lambda^2}{2\beta}\left(\frac{\pi}{2\left(\mathrm{i}v_\psi\right)^d}\csc\frac{\pi d}{2}S_d\right)\sum_{\mathrm{i}\Omega}\frac{\chi_0}{(aT-\mathrm{i}\Omega)^\alpha}\left|\mathrm{i}\omega-\mathrm{i}\Omega-\Sigma_{\psi,\tau}(\mathrm{i}\omega-\mathrm{i}\Omega)\right|^{d-1},\\ \Sigma_{\chi,i} &= 0.\end{aligned} \tag{65}$$

Substituting the power-law form of the self energies, we obtain their explicit expressions as follows

$$C_\psi|\omega|^{\alpha_\psi} = -\frac{\lambda^2}{2\beta}\sum_{\mathrm{i}\Omega}\frac{\chi_0}{(aT-\mathrm{i}\Omega)^\alpha}\frac{1}{\mathrm{i}\omega-\mathrm{i}\Omega-C_\chi|\omega-\Omega|^{\alpha_\chi}} \approx -\frac{\lambda^2}{2\beta}\sum_{\mathrm{i}\Omega}\frac{\chi_0}{(aT-\mathrm{i}\Omega)^\alpha}\frac{1}{C_\chi|\omega-\Omega|^{\alpha_\chi}}, \tag{66}$$

$$\begin{aligned}C_\chi|\omega|^{\alpha_\chi} &= -\frac{\lambda^2}{2\beta}\left(\frac{\pi}{2\left(\mathrm{i}v_\psi\right)^d}\csc\frac{\pi d}{2}S_d\right)\sum_{\mathrm{i}\Omega}\frac{\chi_0}{(aT-\mathrm{i}\Omega)^\alpha}\left|\mathrm{i}\omega-\mathrm{i}\Omega-\Sigma_{\psi,\tau}(\mathrm{i}\omega-\mathrm{i}\Omega)\right|^{d-1}\\ &\approx -\frac{\lambda^2}{2\beta}\left(\frac{\pi}{2\left(\mathrm{i}v_\psi\right)^d}\csc\frac{\pi d}{2}S_d\right)\sum_{\mathrm{i}\Omega}\frac{\chi_0}{(aT-\mathrm{i}\Omega)^\alpha}C_\psi^{d-1}|\omega-\Omega|^{(d-1)\alpha_\psi}.\end{aligned} \tag{67}$$

The self-consistenct condition for the renormalized local susceptibility is

$$\begin{aligned}\chi_{\mathrm{LQCP}}(\mathrm{i}\omega) &= \frac{1}{\beta}\sum_{\mathrm{i}\omega'}\int\frac{d^dk}{(2\pi)^d}\ \mathrm{Tr}\ \mathcal{g}_\chi(\mathrm{i}\omega',\mathbf{k})\mathcal{g}_\psi(\mathrm{i}\omega'+\mathrm{i}\omega,\mathbf{k}+\mathbf{q})\\ &= \frac{2}{\beta}\sum_{\mathrm{i}\omega'}\int\frac{d^dk}{(2\pi)^d}\frac{1}{\mathrm{i}\omega'-\Sigma_{\chi,\tau}(\mathrm{i}\omega')}\frac{\mathrm{i}\omega'+\mathrm{i}\omega-\Sigma_{\psi,\tau}(\mathrm{i}\omega'+\mathrm{i}\omega)}{\left(\mathrm{i}\omega'+\mathrm{i}\omega-\Sigma_{\psi,\tau}(\mathrm{i}\omega'+\mathrm{i}\omega)\right)^2+\left(\mathrm{i}v_\psi k_i\right)^2}.\end{aligned} \tag{68}$$

Performing the momentum integral and substituting the power-law form of the self energies and the spin susceptibility, we have

$$\frac{\chi_0}{(aT-\mathrm{i}\omega)^\alpha} \approx -\frac{2}{\beta}\left(\frac{\pi}{2\left(\mathrm{i}v_\psi\right)^d}\csc\frac{\pi d}{2}S_d\right)\sum_{\mathrm{i}\omega'}\frac{1}{C_\chi|\omega'|^{\alpha_\chi}}C_\psi^{d-1}|\omega'+\omega|^{(d-1)\alpha_\psi}. \tag{69}$$

To obtain the ω/T-scaling, the power of T should be matched in Eqs. (60), (61), and (68). As a result, we find the self-consistent condition for all the critical exponents of the power-law behaviors in frequency

$$\alpha_\psi = 1 - \alpha - \alpha_\chi, \qquad \alpha_\chi = 1 - \alpha + (d-1)\alpha_\psi, \qquad -\alpha = 1 - \alpha_\chi + (d-1)\alpha_\psi. \tag{70}$$

Solving these equations with $d = 2$, we obtain

$$\alpha_\psi = 0, \qquad \alpha_\chi = 1, \qquad \alpha = 0. \tag{71}$$

Indeed, these critical exponents cannot explain our experiments and the phenomenological analysis above. However, this failure should be regarded as an artifact of the one-loop level analysis. The unitarity of this system has to give positive critical exponents for both α_ψ and α [23, 24, 25]. If we introduce the flavor degeneracy N for both fermion excitations and take the large N limit as a theoretical device for a controllable approximation, the next leading order quantum corrections are in the order of $1/N$. It is beyond the scope of the present theoretical analysis to find such critical exponents with the introduction of vertex corrections. However, we claim that the appearance of $1/N$ quantum corrections to the critical exponent α supports why it is quite small compared to the dynamics of decoupled local magnetic moments. The present dynamical mean-field theory analysis at least confirms existence of the heavy-fermion-like local quantum criticality at low energies involving the emergent local dynamics of both Z_2 flux and Ising AFM fluctuations.

C. Calculation details

1. Self-energy and vertex corrections

The self-energy correction for the Ψ-field is given by

$$\begin{aligned}
\Sigma_\Psi(k) &= g^2 \int_{\frac{\Lambda}{b}}^{\Lambda} \frac{d^D q}{(2\pi)^D} \frac{1}{q^2} \frac{-\mathrm{i}\gamma\cdot(k+q+M)}{(k+q+M)^2} \\
&= g^2 \int_{\frac{\Lambda}{b}}^{\Lambda} \frac{d^D q}{(2\pi)^D} \int_0^1 ds\, \frac{-\mathrm{i}\gamma\cdot(k+q+M)}{[q+s(k+M)]^2} \\
&\approx g^2 \int_{\frac{\Lambda}{b}}^{\Lambda} \frac{d^D q}{(2\pi)^D} \int_0^1 ds\, \frac{-\mathrm{i}\gamma\cdot[(1-s)k+M]}{(q+sM)^2} \\
&= -A_\Psi(g,M;\Lambda)\mathrm{i}\gamma\cdot k - A_M(g,M;\Lambda)\,\mathrm{i}\gamma\cdot M,
\end{aligned} \tag{72}$$

where the renormalization coefficients are

$$\begin{aligned}
A_\Psi(g,M;\Lambda) &= g^2 \frac{\pi^{\frac{D}{2}}}{(2\pi)^D \Gamma\left(\frac{D}{2}\right)} F_D^\Psi(M) \frac{dl}{\Lambda^{4-D}}, \\
F_D^\Psi(M) &= \frac{2}{\sqrt{\pi}} \frac{\Gamma\left(\frac{D}{2}\right)}{\Gamma\left(\frac{D-1}{2}\right)} \int_0^1 ds \int_0^\pi d\phi\, \frac{(1-s)\sin^{D-2}\phi}{\left(1+\frac{sM^2}{\Lambda^2}+\frac{2sM}{\Lambda}\cos\phi\right)^2}, \\
A_M(g,M;\Lambda) &= g^2 \frac{\pi^{\frac{D}{2}}}{(2\pi)^D \Gamma\left(\frac{D}{2}\right)} G_D^M(M) \frac{dl}{\Lambda^{4-D}}, \\
G_D^M(M) &= \frac{2}{\sqrt{\pi}} \frac{\Gamma\left(\frac{D}{2}\right)}{\Gamma\left(\frac{D-1}{2}\right)} \int_0^1 ds \int_0^\pi d\phi\, \frac{\sin^{D-2}\phi}{\left(1+\frac{sM^2}{\Lambda^2}+\frac{2sM}{\Lambda}\cos\phi\right)^2}.
\end{aligned} \tag{73}$$

Here, the generalized polar coordinate in a D-dimension has been used. We note that $\delta\Lambda = \Lambda - \Lambda/b = \Lambda dl$, $F_D^\Psi(M=0) = 1$, and $G_D^M(M=0) = 1$.

Similarly, the self-energy correction for the X-field is given by

$$\Sigma_X(k) = g^2 \int_\Lambda \frac{d^D q}{(2\pi)^D} \frac{1}{q^2} \frac{-\mathrm{i}\gamma \cdot (k+q)}{(k+q)^2} \approx -A_X(g, M; \Lambda)\, \mathrm{i}\gamma \cdot k, \tag{74}$$

where the renormalization coefficient is

$$A_X(g, M; \Lambda) = g^2 \frac{\pi^{\frac{D}{2}}}{(2\pi)^D \Gamma\left(\frac{D}{2}\right)} \frac{dl}{\Lambda^{4-D}}. \tag{75}$$

Renoralization of M, the so-called mass renormalization, is irrelevant to Σ_X and is caused by Σ_Ψ. To show this renormalization, we introduce $\mathrm{i}\gamma \cdot M_\Psi$ in the Ψ sector. Then, the self-energy of the X-field is the same as that of the Ψ-field by replacing M with M_Ψ. Demanding $M_{\Psi,\mathrm{ren}} \equiv M_\Psi + \delta M_\Psi = 0$, we have the renormalization as $M \to M - A_M M$.

The self-energy correction for the ϕ-field is given by

$$\Sigma_\phi^{(1)} = -g^2 \int_{\frac{\Lambda}{b}}^{\Lambda} \frac{d^D q}{(2\pi)^D} \mathrm{Tr}\left[\frac{-\mathrm{i}\gamma \cdot q}{q^2} \frac{-\mathrm{i}\gamma \cdot (k+q+M)}{(k+q+M)^2}\right] = g^2 \int_{\frac{\Lambda}{b}}^{\Lambda} \frac{d^D q}{(2\pi)^D} \int_0^1 ds\, \frac{q \cdot (q+k+M)}{[q+s(k+M)]^2}. \tag{76}$$

Expanding $\Sigma_\phi^{(1)}(k)$ in terms of k^2, we have the field renormalization of the form $-A_\phi(g, M; \Lambda)\, k^2$, where

$$A_\phi(g, M; \Lambda) = g^2 \frac{\pi^{\frac{D}{2}}}{(2\pi)^D \Gamma\left(\frac{D}{2}\right)} (\mathrm{Tr}1)\, F_D^\phi(M) \frac{dl}{\Lambda^{4-D}},$$

$$F_D^\phi(M) = \frac{2}{\sqrt{\pi}} \frac{\Gamma\left(\frac{D}{2}\right)}{\Gamma\left(\frac{D-1}{2}\right)} \int_0^1 ds \int_0^\pi d\phi\, \sin^{D-2}\phi \frac{3s(1-s) + s^2(1-s)\frac{M^2}{\Lambda^2} + 2s(1-s^2)\frac{M}{\Lambda}\cos\phi}{\left(1 + \frac{sM^2}{\Lambda^2} + \frac{2sM}{\Lambda}\cos\phi\right)^2}. \tag{77}$$

We note that $F_D^\phi(M=0) = 1$. The self-energy correction due to the λ-coupling effect is given by

$$\Sigma_\phi^{(2)} = -\lambda \int_{\frac{\Lambda}{b}}^{\Lambda} \frac{d^D q}{(2\pi)^D} \frac{1}{q^2}, \tag{78}$$

which does not cause the field renormalization in this one-loop level.

The three-point vertex correction for the coupling constant g is given by

$$\Gamma_g(k, k+q, q) = \mathrm{i}g^3 \int_{\frac{\Lambda}{b}}^{\Lambda} \frac{d^D q'}{(2\pi)^D} \frac{1}{q'^2} \frac{-\mathrm{i}\gamma \cdot (k+q+q')}{(k+q+q')^2} \frac{-\mathrm{i}\gamma \cdot (k+q'+M)}{(k+q'+M)^2}. \tag{79}$$

Here, we set $k = q = 0$ for all external momenta and perform the integral

$$\begin{aligned}\Gamma_g(0,0,0) &= \mathrm{i}g^3 \int_{\frac{\Lambda}{b}}^{\Lambda} \frac{d^D q'}{(2\pi)^D} \frac{1}{q'^2} \frac{-\mathrm{i}\gamma \cdot q'}{q'^2} \frac{-\mathrm{i}\gamma \cdot (q'+M)}{(q'+M)^2} \\ &= -2\mathrm{i}g^3 \int_0^1 ds \int \frac{d^D q'}{(2\pi)^D} \frac{s(q'^2 + \gamma \cdot q'\, \gamma \cdot M)}{\{[q' + (1-s)M]^2 + s(1-s)M^2\}^3}.\end{aligned} \tag{80}$$

For this Γ_g vertex correction, we have to consider a term proportional to the unit matrix in the spinor space. Taking into account $\gamma_i \gamma_j \to \gamma_i \gamma_i$, we obtain

$$
\begin{aligned}
\Gamma_g(0,0,0) &\to -2\mathrm{i}g^3\int_0^1 ds\int_{\frac{\Lambda}{b}}^{\Lambda}\frac{d^Dq'}{(2\pi)^D}\,\frac{(1-s)(q'^2+q'\cdot M)}{(q'^2+2sM\cdot q'+sM^2)^3} \\
&\approx -2\mathrm{i}g^3\,\frac{\pi^{\frac{D}{2}}}{(2\pi)^D\Gamma\left(\frac{D}{2}\right)}G_D^g(M)\,\frac{dl}{\Lambda^{4-D}},
\end{aligned}
\tag{81}
$$

where the renormalization coefficient is

$$
G_D^g(M)=\frac{2}{\sqrt{\pi}}\frac{\Gamma\left(\frac{D}{2}\right)}{\Gamma\left(\frac{D-1}{2}\right)}\int_0^1 ds\int_0^{\pi}d\phi\,\frac{(1-s)\sin^{D-2}\phi\left(1+\frac{M}{\Lambda}\cos\phi\right)}{\left(1+\frac{sM^2}{\Lambda^2}+\frac{2sM}{\Lambda}\cos\phi\right)^3}. \tag{82}
$$

We note that $G_D(M=0)=1$.

The four-point vertex correction for the coupling constant λ is given by

$$
\Gamma_\lambda^{(1)}=-\frac{3\lambda^2}{2}\int_{\frac{\Lambda}{b}}^{\Lambda}\frac{d^Dq}{(2\pi)^D}\frac{1}{(q^2)^2}\approx-\frac{3\lambda^2}{2}\frac{2\pi^{\frac{D}{2}}}{(2\pi)^D\Gamma\left(\frac{D}{2}\right)}\frac{dl}{\Lambda^{4-D}}, \tag{83}
$$

as well known [16].

The three-point interaction vertex gives rise to renormalization for the four-point self-interaction vertex as follows

$$
\begin{aligned}
\Gamma_\lambda^{(2)} &= 12g^4\int_{\frac{\Lambda}{b}}^{\Lambda}\frac{d^Dq}{(2\pi)^D}\,\mathrm{Tr}\frac{-\mathrm{i}\gamma\cdot(q+M)}{(q+M)^2}\frac{-\mathrm{i}\gamma\cdot q}{q^2}\frac{\mathrm{i}\gamma\cdot(q+M)}{(q+M)^2}\frac{-\mathrm{i}\gamma\cdot q}{q^2} \\
&= 24g^4\int_{\frac{\Lambda}{b}}^{\Lambda}\frac{d^Dq}{(2\pi)^D}\,\frac{q^4+2(M\cdot q)q^2+2(M\cdot q)^2-M^2q^2}{q^4(q+M)^4} \\
&= 24g^4\int_0^1 ds\int_{\frac{\Lambda}{b}}^{\Lambda}\frac{d^Dq}{(2\pi)^D}\,s(1-s)\frac{q^4+2(M\cdot q)q^2+2(M\cdot q)^2-M^2q^2}{(q^2+sM^2+2sM\cdot q)^4} \\
&= 24g^4\frac{2\pi^{\frac{D-1}{2}}}{(2\pi)^D\Gamma\left(\frac{D-1}{2}\right)}\frac{dl}{\Lambda^{4-D}}\int_0^1 ds\int_0^{\pi}d\phi\,s(1-s)\sin^{D-2}\phi\frac{1+\frac{2M}{\Lambda}\cos\phi+\frac{2M^2}{\Lambda^2}\cos^2\phi-\frac{M^2}{\Lambda^2}}{\left(1+\frac{sM^2}{\Lambda^2}+\frac{2sM}{\Lambda}\cos\phi\right)^4} \\
&= 24g^4\frac{\pi^{\frac{D}{2}}}{(2\pi)^D\Gamma\left(\frac{D}{2}\right)}G_D^\lambda(M)\frac{dl}{\Lambda^{4-D}}.
\end{aligned}
\tag{84}
$$

Here, we have

$$
G_D^\lambda(M)=\frac{2}{\sqrt{\pi}}\frac{\Gamma\left(\frac{D}{2}\right)}{\Gamma\left(\frac{D-1}{2}\right)}\int_0^1 ds\int_0^{\pi}d\phi\,s(1-s)\sin^{D-2}\phi\frac{1+\frac{2M}{\Lambda}\cos\phi+\frac{2M^2}{\Lambda^2}\cos^2\phi-\frac{M^2}{\Lambda^2}}{\left(1+\frac{sM^2}{\Lambda^2}+\frac{2sM}{\Lambda}\cos\phi\right)^4}. \tag{85}
$$

2. Dynamic spin susceptibility

The Γ-point spin susceptibility is given by

$$\chi_\Gamma^{(0)}(\mathrm{i}\nu,\mathbf{q}) = -\frac{1}{\beta}\sum_{\mathrm{i}\omega}\int \frac{d^2k}{(2\pi)^2}\,\mathrm{Tr}\left[\frac{-\mathrm{i}\gamma_0(\omega+\nu)-\mathrm{i}\boldsymbol{\gamma}\cdot(\mathbf{k}+\mathbf{q}+\mathbf{M})}{(\omega+\nu)^2+(\mathbf{k}+\mathbf{q}+\mathbf{M})^2}\gamma_0\frac{-\mathrm{i}\gamma_0\omega-\mathrm{i}\boldsymbol{\gamma}\cdot\boldsymbol{k}}{\omega^2+\mathbf{k}^2}\gamma_0\right] + (q \to -q)$$
$$= -\frac{2}{\beta}\sum_{\mathrm{i}\omega}\int \frac{d^2k}{(2\pi)^2}\frac{\mathrm{i}\omega(\mathrm{i}\omega+\mathrm{i}\nu)+\mathbf{k}\cdot(\mathbf{k}+\mathbf{q}+\mathbf{M})}{[(\mathrm{i}\omega)^2-\mathbf{k}^2][(\mathrm{i}\omega+\mathrm{i}\nu)^2-(\mathbf{k}+\mathbf{q}+\mathbf{M})^2]} + (q\to -q). \tag{86}$$

Performing the Matsubara frequency summation, we obtain

$$-\frac{1}{\beta}\sum_{\mathrm{i}\omega}\frac{\mathrm{i}\omega(\mathrm{i}\omega+\mathrm{i}\nu)+\mathbf{k}\cdot(\mathbf{k}+\mathbf{q}+\mathbf{M})}{[(\mathrm{i}\omega)^2-\vec{k}^2][(\mathrm{i}\omega+\mathrm{i}\nu)^2-(\mathbf{k}+\mathbf{q}+\mathbf{M})^2]}$$
$$= -\frac{1}{4}\left(1+\frac{\mathbf{k}\cdot(\mathbf{k}+\mathbf{q}+\mathbf{M})}{|\mathbf{k}||\mathbf{k}+\mathbf{q}+\mathbf{M}|}\right)\left[\frac{f(|\mathbf{k}|)-f(|\mathbf{k}+\mathbf{q}+\mathbf{M}|)}{\mathrm{i}\nu+|\mathbf{k}|-|\mathbf{k}+\mathbf{q}+\mathbf{M}|}+\frac{f(-|\mathbf{k}|)-f(-|\mathbf{k}+\mathbf{q}+\mathbf{M}|)}{\mathrm{i}\nu-|\mathbf{k}|+|\mathbf{k}+\mathbf{q}+\mathbf{M}|}\right]$$
$$-\frac{1}{4}\left(1-\frac{\mathbf{k}\cdot(\mathbf{k}+\mathbf{q}+\mathbf{M})}{|\mathbf{k}||\mathbf{k}+\mathbf{q}+\mathbf{M}|}\right)\left[\frac{f(|\mathbf{k}|)-f(-|\mathbf{k}+\mathbf{q}+\mathbf{M}|)}{\mathrm{i}\nu+|\mathbf{k}|+|\mathbf{k}+\mathbf{q}+\mathbf{M}|}+\frac{f(-|\mathbf{k}|)-f(|\mathbf{k}+\mathbf{q}+\mathbf{M}|)}{\mathrm{i}\nu-|\mathbf{k}|-|\mathbf{k}+\mathbf{q}+\mathbf{M}|}\right]. \tag{87}$$

As a result, we find

$$\chi_\Gamma^{(0)}(\mathrm{i}\nu,\mathbf{q}) = -\frac{1}{2}\int\frac{d^2k}{(2\pi)^2}\left(1+\frac{\mathbf{k}\cdot(\mathbf{k}+\mathbf{q}+\mathbf{M})}{|\mathbf{k}||\mathbf{k}+\mathbf{q}+\mathbf{M}|}\right)\left[\frac{f(|\mathbf{k}|)-f(|\mathbf{k}+\mathbf{q}+\mathbf{M}|)}{\mathrm{i}\nu+|\mathbf{k}|-|\mathbf{k}+\mathbf{q}+\mathbf{M}|}+\frac{f(-|\mathbf{k}|)-f(-|\mathbf{k}+\mathbf{q}+\mathbf{M}|)}{\mathrm{i}\nu-|\mathbf{k}|+|\mathbf{k}+\mathbf{q}+\mathbf{M}|}\right]$$
$$-\frac{1}{2}\int\frac{d^2k}{(2\pi)^2}\left(1-\frac{\mathbf{k}\cdot(\mathbf{k}+\mathbf{q}+\mathbf{M})}{|\mathbf{k}||\mathbf{k}+\mathbf{q}+\mathbf{M}|}\right)\left[\frac{f(|\mathbf{k}|)-f(-|\mathbf{k}+\mathbf{q}+\mathbf{M}|)}{\mathrm{i}\nu+|\mathbf{k}|+|\mathbf{k}+\mathbf{q}+\mathbf{M}|}+\frac{f(-|\mathbf{k}|)-f(|\mathbf{k}+\mathbf{q}+\mathbf{M}|)}{\mathrm{i}\nu-|\mathbf{k}|-|\mathbf{k}+\mathbf{q}+\mathbf{M}|}\right] + (q\to -q). \tag{88}$$

Taking into account $\mathrm{i}\nu \to \nu + \mathrm{i}\delta$ and the limit of $q \to 0$, we obtain

$$\chi_\Gamma^{\mathrm{ret},(0)}(\nu,\mathbf{q}=0)$$
$$= -\frac{1}{4\pi^2}\int_0^\infty dk\int_0^{2\pi}d\theta\,k\left(1+\frac{k+M\cos\theta}{k_M}\right)\left[\frac{f(k)-f(k_M)}{\nu+k-k_M+\mathrm{i}\delta}+\frac{f(-k)-f(-k_M)}{\nu-k+k_M+\mathrm{i}\delta}\right]$$
$$-\frac{1}{4\pi^2}\int_0^\infty dk\int_0^{2\pi}d\theta\,k\left(1-\frac{k+M\cos\theta}{k_M}\right)\left[\frac{f(k)-f(-k_M)}{\nu+k+k_M+\mathrm{i}\delta}+\frac{f(-k)-f(k_M)}{\nu-k-k_M+\mathrm{i}\delta}\right], \tag{89}$$

where the short-hand notation is $k_M = \sqrt{k^2+M^2+2Mk\cos\theta}$.

It is straightforward to extract out the imaginary part

$$\mathrm{Im}\chi_\Gamma^{\mathrm{ret},(0)}(\nu,\mathbf{q}=0)$$
$$= \frac{1}{4\pi}\int_0^\infty dk\int_0^{2\pi}d\theta\,k\left(1+\frac{k+M\cos\theta}{k_M}\right)[f(k)-f(k_M)]\delta(\nu+k-k_M)$$
$$+\frac{1}{4\pi}\int_0^\infty dk\int_0^{2\pi}d\theta\,k\left(1+\frac{k+M\cos\theta}{k_M}\right)[f(-k)-f(-k_M)]\delta(\nu-k+k_M)$$
$$+\frac{1}{4\pi}\int_0^\infty dk\int_0^{2\pi}d\theta\,k\left(1-\frac{k+M\cos\theta}{k_M}\right)[f(k)-f(-k_M)]\delta(\nu+k+k_M)$$
$$+\frac{1}{4\pi}\int_0^\infty dk\int_0^{2\pi}d\theta\,k\left(1-\frac{k+M\cos\theta}{k_M}\right)[f(-k)-f(k_M)]\delta(\nu-k-k_M). \tag{90}$$

Without any loss of generality, we consider $\nu > 0$. Then, we have

$$
\begin{aligned}
&\mathrm{Im}\chi_{\Gamma}^{\mathrm{ret},(0)}(\nu,\mathbf{q}=0) \\
&= \frac{1}{2\pi}\int_0^\infty dk \int_0^\pi d\theta\, k \frac{\nu + 2k + M\cos\theta}{\nu + k}[f(k) - f(k+\nu)]\delta(\nu + k - k_M) \\
&+ \frac{1}{2\pi}\int_0^\infty dk \int_0^\pi d\theta\, k \frac{\nu - 2k - M\cos\theta}{\nu - k}[f(-k) - f(-k+\nu)]\delta(\nu - k + k_M) \\
&+ \frac{1}{2\pi}\int_0^\infty dk \int_0^\pi d\theta\, k \frac{\nu - 2k - M\cos\theta}{\nu - k}[f(-k) - f(-k+\nu)]\delta(\nu - k - k_M).
\end{aligned}
\tag{91}
$$

First, we consider $\nu > M$. Then, the first and the second delta functions are zero. As a result, we find

$$
\begin{aligned}
&\mathrm{Im}\chi_{\Gamma}^{\mathrm{ret},(0)}(\nu,\mathbf{q}=0) \\
&\qquad = \frac{1}{2\pi}\int_0^\infty dk \int_0^\pi d\theta\, k \frac{\nu - 2k - M\cos\theta}{\nu - k}[f(-k) - f(-k+\nu)]\delta(\nu - k - k_M).
\end{aligned}
\tag{92}
$$

Performing the θ-integration, we obtain

$$
\mathrm{Im}\chi_{\Gamma}^{\mathrm{ret},(0)}(\nu,\mathbf{q}=0) = \frac{1}{4\pi}\int_{\nu-M2}^{\nu+M2} dk \sqrt{\frac{M^2 - (2k-\nu)^2}{\nu^2 - M^2}}\left(\tanh\frac{k}{2T} - \tanh\frac{k-\nu}{2T}\right).
\tag{93}
$$

Second, we consider $\nu < M$. Then, the third delta function is zero. As a result, we find

$$
\begin{aligned}
&\mathrm{Im}\chi_{\Gamma}^{\mathrm{ret},(0)}(\nu,\mathbf{q}=0) \\
&= \frac{1}{2\pi}\int_{M-\nu}^\infty dk\, \frac{\nu + 2k + M\cos\theta_1}{M\sin\theta_1}\,[f(k) - f(k+\nu)] + \frac{1}{2\pi}\int_{M+\nu}^\infty dk\, \frac{-\nu + 2k + M\cos\theta_2}{M\sin\theta_2}\,[f(-k) \\
&\qquad - f(-k+\nu)] \\
&= \frac{1}{4\pi}\int_{M-\nu}^\infty dk \sqrt{\frac{(2k+\nu)^2 - M^2}{M^2 - \nu^2}}\left(\tanh\frac{k+\nu}{2T} - \tanh\frac{k}{2T}\right) \\
&\qquad + \frac{1}{4\pi}\int_{M+\nu}^\infty dk \sqrt{\frac{(2k-\nu)^2 - M^2}{M^2 - \nu^2}}\left(\tanh\frac{k}{2T} - \tanh\frac{k-\nu}{2T}\right),
\end{aligned}
\tag{94}
$$

where $\cos\theta_1 = \frac{(\nu+k)^2 - M^2 - k^2}{2Mk}$ and $\cos\theta_2 = \frac{(\nu-k)^2 - M^2 - k^2}{2Mk} = \cos\theta_0$.

Supplementary References

[1] S.-H. Do, S.-Y. Park, J. Yoshitake, J. Nasu, Y. Motome, Y. Kwon, D. Adroja, D. Voneshen, K. Kim, T.-H. Jang, J.-H. Park, K.-Y. Choi, and S. Ji, "Majorana fermions in the Kitaev quantum spin system α-$RuCl_3$," *Nature Phys.* **13**, 1079-1084 (2017).

[2] R. A. Ewings, A. Buts, M. D. Le, J. v. Duijn, I. Bustinduy, and T. G. Perring, "Horace: Software for the analysis of data from single crystal spectroscopy experiments at time-of-flight neutron instruments," *Nucl. Instrum. Methods Phys. Res. A: Accel. Spectrometers, Detect. Assoc. Equip.* **834**, 132-142 (2016).

[3] H. Li, T. T. Zhang, A. Said, G. Fabbris, D. G. Mazzone, J. Q. Yan, D. Mandrus, G. B. Halász, S. Okamoto, S. Murakami, M. P. M. Dean, H. N. Lee, and H. Miao, "Giant phonon anomalies in the proximate Kitaev quantum spin liquid α-$RuCl_3$," *Nat. Commun.* **12**, 3513 (2021).

[4] K. A. Modic, R. D. McDonald, J. P. C. Ruff, M. D. Bachmann, Y. Lai, J. C. Palmstrom, D. Graf, M. K. Chan, F. F. Balakirev, J. B. Betts, G. S. Boebinger, M. Schmidt, M. J. Lawler, D. A. Sokolov, P. J. W. Moll, B. J. Ramshaw, and A. Shekhter, "Scale-invariant magnetic anisotropy in $RuCl_3$ at high magnetic fields," *Nat. Phys* **17**, 240-244 (2021).

[5] J. Chaloupka and G. Khaliullin, "Magnetic anisotropy in the Kitaev model systems Na_2IrO_3 and $RuCl_3$," *Phys. Rev. B* **94**, 064435 (2016).

[6] P. Laurell and S. Okamoto, "Dynamical and thermal magnetic properties of the Kitaev spin liquid candidate α-$RuCl_3$," *npj Quantum Mater.* **5**, 2 (2020).

[7] M. Bouvier, P. Lethuillier, and D. Schmitt, "Specific heat in some gadolinium compounds. I. Experimental," *Phys. Rev. B* **43**, 13137 (1991).

[8] A. Kitaev, "Anyons in an exactly solved model and beyond," *Ann. Phys.* **321**, 2-11 (2006).

[9] H. Cao, A. Banerjee, J.-Q. Yan, C. Bridges, M. Lumsden, D. Mandrus, D. Tennant, B. Chakoumakos, and S. Nagler, "Low-temperature crystal and magnetic structure of α-$RuCl_3$," *Phys. Rev. B* **93**, 134423 (2016).

[10] R. Johnson, S. Williams, A. Haghighirad, J. Singleton, V. Zapf, P. Manuel, I. Mazin, Y. Li, H. Jeschke, R. Valentí, and R. Coldea, "Monoclinic crystal structure of α-$RuCl_3$ and the zigzag antiferromagnetic ground state," *Phys. Rev. B* **92**, 235119 (2015).

[11] S.-Y. Park, S.-H. Do, K.-Y. Choi, D. Jang, T.-H. Jang, J. Schefer, C.-M. Wu, J. Gardner, J. Park, J.-H. Park, and S. Ji, "Emergence of the Isotropic Kitaev Honeycomb Lattice with Two-dimensional Ising Universality in α-$RuCl_3$," arXiv:1609.05690 (2016).

[12] K. Ran, J. Wang, W. Wang, Z.-Y. Dong, X. Ren, S. Bao, S. Li, Z. Ma, Y. Gan, Y. Zhang, J. Park, G. Deng, S. Danilkin, S.-L. Yu, J.-X. Li, and J. Wen, "Spin-Wave Excitations Evidencing the Kitaev Interaction in Single Crystalline α−$RuCl_3$," *Phys. Rev. Lett.* **118**, 107203 (2017).

[13] H.-D. Chen and Z. Nussinov, "Exact results of the Kitaev model on a hexagonal lattice: spin states, string and brane correlators, and anyonic excitations," *J. Phys. A: Math. Theor.* **41**, 075001 (2008).

[14] D.-H. Lee, G.-M. Zhang, and T. Xiang, "Edge Solitons of Topological Insulators and Fractionalized Quasiparticles in Two Dimensions," *Phys. Rev. Lett.* **99**, 196805 (2007).

[15] A. Gogolin, A. Nersesyan, and A. Tsvelik, Bosonization and strongly correlated systems, Cambridge University Press, 1998.

[16] J. Zinn-Justin, Quantum field theory and critical phenomena, 4th edn., New York: Clarendon Press, 2002.

[17] K. Wilson, "Quantum Field - Theory Models in Less Than 4 Dimensions," *Phys. Rev. D* **7**, 2911 (1973).

[18] J. Gonzáleza, F. Guineab, and M. Vozmedianoc, "Non-Fermi liquid behavior of electrons in the half-filled honeycomb lattice (A renormalization group approach)," *Nucl. Phys. B* **424**, 595-618 (1994).

[19] N. Nagaosa, Quantum Field Theory in Strongly Correlated Electron Systems, Springer, 1999.

[20] A. Schröder, G. Aeppli, R. Coldea, M. Adams, O. Stockert, H. Löhneysen, E. Bucher, R. Ramazashvili, and P. Coleman, "Onset of antiferromagnetism in heavy-fermion metals," *Nature* **407**, 351-355 (2000).

[21] O. Parcollet, A. Georges, G. Kotliar, and A. Sengupta, "Overscreened multichannel SU(N) Kondo model: Large-N solution and conformal field theory," *Phys. Rev. B* **58**, 3794 (1998).

[22] E. Müller-Hartmann, "Self-consistent perturbation theory of the anderson model: Ground state properties," *Z. Phys. B* **57**, 281 (1984).

[23] S. Ferrara, A. Grillo, R. Gatto, and G. Parisi, "Analyticity properties and asymptotic expansions of conformal covariant Green's functions," *Nuovo Cimento A* **19**, 667–695 (1974).

[24] S. Minwalla, "Restrictions imposed by superconformal invariance on quantum field theories," *Adv. Theor. Math. Phys.* **2**, 781 (1998).

[25] D. Poland, S. Rychkov, and A. Vichi, "The conformal bootstrap: Theory, numerical techniques, and applications," *Rev. Mod. Phys.* **91**, 015002 (2019).